

WAS COMET C/1945 X1 (DU TOIT) A DWARF, *SOHO*-LIKE KREUTZ SUNGRAZER?

ZDENEK SEKANINA¹ & RAINER KRACHT²

¹Jet Propulsion Laboratory, California Institute of Technology, 4800 Oak Grove Drive, Pasadena, CA 91109, U.S.A.

²Ostlandring 53, D-25335 Elmshorn, Schleswig-Holstein, Germany

Version September 9, 2021

ABSTRACT

The goal of this investigation is to reinterpret and upgrade the astrometric and other data on comet C/1945 X1, the least prominent among the Kreutz system sungrazers discovered from the ground in the 20th century. The central issue is to appraise the pros and cons of a possibility that this object is — despite its brightness reported at discovery — a dwarf Kreutz sungrazer. We confirm Marsden’s (1989) conclusion that C/1945 X1 has a common parent with C/1882 R1 and C/1965 S1, in line with the Sekanina-Chodas (2004) scenario of their origin in the framework of the Kreutz system’s evolution. We integrate the orbit of C/1882 R1 back to the early 12th century and then forward to around 1945 to determine the nominal direction of the line of apsides and perform a Fourier analysis to get insight into effects of the indirect planetary perturbations. To better understand the nature of C/1945 X1, its orbital motion, fate, and role in the hierarchy of the Kreutz system, as well as to attempt detecting the comet’s possible terminal outburst shortly after perihelion and answer the question in the title of this investigation, we closely examined the relevant Boyden Observatory logbooks and identified both the photographs with the comet’s known images and nearly 20 additional patrol plates, taken both before and after perihelion, on which the comet or traces of its debris will be searched for, once the process of their digitization, currently conducted as part of the Harvard College Observatory’s DASCH Project, has been completed and the scanned copies made available to the scientific community.

Subject headings: comets: general — methods: data analysis

1. INTRODUCTION

As the most extensive system of genetically related comets in existence, the Kreutz sungrazers represent an inexhaustible source of research opportunities. Kreutz’s (1888, 1891, 1901) celebrated orbital studies described the motions of the early bright members, showing that they moved about the Sun in similar, extraordinarily elongated paths, with orbital periods of up to about 1000 yr, yet approaching the Sun’s surface to within one solar radius at perihelion. Kreutz’s work was followed by many more studies in the 20th century, with those by Marsden (1967, 1989) standing out as the most important.

Because all Kreutz sungrazers are fragments of one progenitor, their orbits’ lines of apsides are nearly perfectly aligned; the scatter is only a small fraction of 1°, a product of indirect perturbations by the planets, Jupiter in particular (Marsden 1967), and of the process of cascading fragmentation (Sekanina 2002). The research on the Kreutz system has recently accelerated explosively thanks to vast new evidence provided by imagers on board the spacecraft dedicated to the exploration of the Sun, especially the coronagraphs C2 and C3 of the *Solar and Heliospheric Observatory* (*SOHO*; see Brueckner et al. 1995) and the coronagraphs COR2 and imagers HI1 of the *Solar Terrestrial Relations Observatory*’s two probes (*STEREO-A* and *B*; see Howard et al. 2008). Over the past two decades, these instruments allowed detection, in close proximity of the Sun, of thousands of minor Kreutz system’s members, referred to hereafter as the *dwarf* sungrazers, which keep streaming toward the Sun but always disintegrate shortly before reaching perihelion.

The directions of the lines of apsides of 1600 dwarf Kreutz sungrazers derived from their published gravitational orbits were recently shown by us (Sekanina & Kracht 2015; hereafter referred to as Paper 1) to be distributed along an arc of 25° (sic!) in the ecliptical latitude, failing utterly to comply with the condition of directional alignment. We determined that this major effect was due to a neglected nongravitational acceleration in the dwarf sungrazers’ motions, which was orders of magnitude greater than the nongravitational accelerations in the motions of the cataloged comets in nearly-parabolic orbits with perihelia a few tenths of AU from the Sun or more, topping in exceptional cases the Sun’s gravitational acceleration. In summary, the *preperihelion disintegration* and a *very high erosion-driven nongravitational acceleration* of the orbital motion are two fundamental attributes of the dwarf Kreutz sungrazers.

2. SUNGRAZING COMET C/1945 X1 (DU TOIT)

On 1945 December 11, a comet was discovered photographically by D. du Toit at the Harvard College Observatory’s Boyden Station near Bloemfontein, South Africa (Paraskevopoulos 1945); nowadays this comet is referred to as C/1945 X1. The object moved rapidly toward the Sun and its brightness at discovery was reported as magnitude 7. Additional plates were taken at Boyden on the following nights until December 15, but the five *estimated* astrometric positions were not communicated until 1946 January 2, when Cunningham (1946a) used them to compute three very preliminary parabolic orbits. They indicated that the comet was apparently a Kreutz sungrazer that had passed perihelion five days before the cable was sent. Cunningham (1946b) pointed out that his search ephemeris, based on one of the three orbits, was uncer-

tain “by many degrees.” Published accounts show that after December 15 the comet was lost and never seen again. Contrary to expectations, it did not become a brilliant object near and/or after perihelion. Its failure to develop a bright headless tail for a limited period of time after perihelion — contrary to such sungrazers as C/1887 B1 (see the references in Sekanina 2002) and C/2011 W3 (e.g., Sekanina & Chodas 2012) — suggests that C/1945 X1 may have disintegrated already before perihelion, as do the dwarf Kreutz sungrazers. This possibility raises a question of whether or not this object was the only dwarf Kreutz sungrazer discovered and repeatedly observed from the ground outside a total solar eclipse.¹ To address this issue in detail requires that three critical points be answered:

(1) Can a very high nongravitational acceleration be conclusively detected in the comet’s orbital motion from the five Boyden observations?

(2) Why was the comet so bright 17 days before perihelion? Was it in outburst or was the reported brightness grossly overestimated?

(3) Was the absence of the comet’s relics after perihelion conditioned on a compelling qualifier or constraint, so that the comet’s preperihelion disintegration could be subject to doubt?

We present new evidence in the following sections that allows us to comment on these points and to chart the lines of attack in the near future.

3. THE BOYDEN PHOTOGRAPHIC OBSERVATIONS

A striking feature of the information on the comet’s Boyden observations is an extremely slow and protracted progress in propagating their results, with an essentially complete lack of details. This is most surprising, given that C/1945 X1 was the first Kreutz sungrazer of the 20th century, after a pause of nearly 60 years.

An emphatic example of the slow progress is the publication of the comet’s astrometry from the Boyden plates. After a delayed message of the estimated positions (whose observation times were announced with a precision to 1 hr!), there was no follow-up report and no computation of an improved orbit until 22 years later, when Marsden (1967), revealing that the plates were measured and reduced by A. G. Mowbray in 1952, derived several sets of parabolic elements. Strangely, these astrometric data were reported by neither Mowbray himself nor L. E. Cunningham, for whom Mowbray was then working (Hockey 2009). In fact, the positions were published only 37 years after they were measured and reduced and 44 years after they were taken by the Boyden observers (Marsden 1989)!

The circumstances of the comet’s observations at Boyden have never been published. We were especially interested in the telescopes or cameras employed to make these photographic observations, in exposure times used, and in the type of tracking (sidereal or on the comet) of the post-discovery photographs. The only information learnt from the literature was that in the 1940s Boyden observers, such as M. J. Bester, discovered their comets

with either the Metcalf 25-cm f/4.9 Triplet refractor or the Bache 20-cm f/5.7 Doublet refractor (Cooper 2003, 2005) while examining plates for image quality.²

As integral part of the Harvard College Observatory’s *Digital Access to a Sky Century@Harvard* (DASCH) Project, all Boyden plates are in the process of being digitized, with the scans gradually made available to the scientific community (Simcoe et al. 2006; Grindlay et al. 2012).³ The products of this effort will eventually play a major role in our quest for information on the comet. Of imminent interest to us are the observing logbooks on the Harvard website; after some search, we have already been able to identify all five plates measured and reduced by Mowbray. Three surprises surfaced: (i) the comet was *not* discovered on a plate taken with the Metcalf or Bache telescope; (ii) a never-reported post-perihelion search was attempted with two instruments on 1946 January 8, 11 days after perihelion and the same day that Cunningham’s (1946b) ephemeris was issued; and (iii) none of the follow-up observations was made by the discoverer.

Table 1 presents the results of our search for the relevant Boyden plates. For each, the individual columns list: the plate number, the UT time of mid-exposure; the approximate equatorial coordinates of the plate center (converted to the equinox J2000); the local sidereal times of the exposure’s start and termination; the resulting exposure time; the logbook reference; and the observer. Three instruments were employed to observe, or search for, the comet: the Metcalf Triplet (plates MF; a plate scale of $167''.3 \text{ mm}^{-1}$) and two small cameras mounted piggyback on the Metcalf, the Cooke 3.8-cm f/8.9 lens (plates AM, including the discovery one; a plate scale of $610''.8 \text{ mm}^{-1}$) and the Ross-Fecker 7.5-cm f/7 camera (plates RB; a plate scale of $395''.5 \text{ mm}^{-1}$). The limiting magnitudes of the three instruments are listed on the Harvard website as, respectively, 17, 13–14, and 15, all much fainter than the comet’s reported magnitude at discovery.

All plates employed for C/1945 X1 had apparently a blue sensitive emulsion (class L; see the DASCH website footnote) and all three instruments used a plate size of 20.3 cm (in right ascension) by 25.4 cm (in declination),⁴ covering fields of $15^\circ:1$ (Metcalf), $35^\circ:7$ (Ross-Fecker), and $55^\circ:2$ (Cooke) in angular extent along a diagonal.

The logbooks show that, of the five observations astrometrically measured and reduced by Mowbray and published by Marsden (1989), the ones on December 11–12 were made with the Cooke lens and only the ones on December 13–15 with the Metcalf refractor. The logbooks further show that the comet was $\sim 12^\circ$ from the center on the discovery plate, $2^\circ:9$ on the December 12 Cooke plate, always less than $1^\circ:2$ on the Metcalf plates, and just about $9^\circ:6$ on the December 14 Cooke plate, which apparently has never been measured. The question of

² These plates were taken on behalf of H. Shapley, Director of the Harvard College Observatory, for the purpose of studying southern variable stars (Cooper 2003, 2005; van Heerden 2008).

³ The DASCH Project, at <http://dasch.rc.fas.harvard.edu/>, involves digitization of more than 500 000 Harvard plates and is currently in progress; see also <http://tdc-www.harvard.edu/plates/>.

⁴ The website <http://tdc-www.harvard.edu/plates/mf/> specifies that Metcalf plates have generally sizes 8 in by 10 in, 14 in by 17 in, and, some early ones, 10 in by 12 in.

¹ A dwarf sungrazer C/2008 O1 was detected during a total solar eclipse on some exposures after a search based on data from *SOHO* (Pasachoff et al. 2009). C/1882 K1 (Tewfik), discovered ~ 3.5 hr preperihelion at $5.6 R_\odot$ (Marsden 1967, 1989) during a total solar eclipse on 1882 May 17, may have been a dwarf sungrazer as well.

Table 1
Boyden Plates with Reported Images or Possible Images of Comet C/1945 X1.

Plate number ^a	UT time at mid-exposure	Plate center ^b		Sidereal time		Exposure time (min)	Logbook reference	Observer ^c
		R.A.	Dec.	start	stop			
AM 25201 ^d	1945 Dec. 11.04709	13 ^h 36 ^m .7	−60° 31′	7 ^h 26 ^m	8 ^h 56 ^m	90	am45b_0158	du Toit
AM 25206	12.04713	15 18.7	−65 22	7 30	9 00	90	am45b_0158	Bester
MF 34987	13.07210	16 19.0	−63 03	8 40	9 10	30	mf25b_0086	Britz
AM 25208 ^e	14.03336	16 40.9	−70 12	7 43	8 23	40	am45b_0158	J(?)
MF 34991	14.05898	16 42.9	−61 12	8 25	8 55	30	mf25b_0086	J(?)
MF 34994	15.06906	17 02.6	−58 39	8 51	9 06	15	mf25b_0088	J(?)
MF 35030	1946 Jan. 8.06517	17 17.5	−47 19	10 05	10 50	45	mf25b_0094	Bester
RB 14184	8.07729	17 17.5	−47 19	10 25	11 05	40	rb10_148	Bester

^a AM plates taken with the Cooke lens; MF plates with the Metcalf telescope; and RB plate with the Ross-Fecker camera.

^b Equinox J2000.

^c The identity of the observer whose abbreviation in the logbooks was J could not be determined; see also Table 12.

^d Discovery plate.

^e This plate appears to have never been astrometrically measured and reduced.

whether or not the comet is located on the plates taken on January 8 can only be answered after our orbital analysis (see Sections 7.1 and 8.2).

4. HISTORY OF THE COMET'S ORBIT DETERMINATION

The sets of orbital elements for comet C/1945 X1 computed by Cunningham (1946a) were much too uncertain to use as a basis of subsequent research. A more accurate orbit was a gravitational parabolic approximation derived by Marsden (1967), who employed the astrometry by Mowbray. Marsden concluded that the December

14 data point (which we found was measured on a MF plate) was inconsistent with the other four positions and he omitted it from what he described as the final set of orbital elements obtained by least squares. The four employed positions were fitted with a mean residual of $\pm 2''.1$, the orbit appeared to be similar to those of C/1882 R1 and C/1965 S1, and ever since 1972 it has been listed, as the representative orbit for C/1945 X1, in the *Catalogue of Cometary Orbits* (see Marsden & Williams 2008 for the most recent edition).

More recently, this comet's orbital motion was further examined by Marsden (1989). He computed four different gravitational solutions, A–D, constraining them to a prescribed orientation of the line of apsides and allowing the orbit to depart from a parabola. His solutions C and D are discussed more extensively in Section 6.1.⁵

In terms of the orientation of the line of apsides, a very stable orbital parameter, the representative orbit of C/1945 X1 is compared in Figure 1 with more reliably determined orbits of seven bright sungrazers. The errors for six of them are smaller than the size of the symbols. For C/1945 X1 the error is estimated by comparing the scatter in the apsidal line with that in the angular elements, combined with the errors of the elements, as published by Marsden (1967). The estimated error for C/1880 C1 is due largely to the uncertainty in the orbital period, as investigated by Kreutz (1901). There is a striking discrepancy between C/1945 X1 and the other sungrazers in Figure 1, exceeding six standard deviations, thus providing grounds for suspecting that the motion of C/1945 X1 might be — like the motions of the dwarf sungrazers — significantly affected by nongravitational forces.

As of now, it has not been demonstrated conclusively whether there exists a purely gravitational orbital solution for C/1945 X1 that simultaneously (i) fits satisfactorily at least four of the five available observations; (ii) complies with the proper orientation of the line of apsides; and (iii) is consistent with a plausible osculating orbital period. Addressing this issue requires in the first place that we know the appropriate values of the quan-

⁵ Marsden (1989) remarked that the December 14 observation was reconstructed for an arbitrarily chosen observation time from the residuals in his previous paper (Marsden 1967), because the original data were unfortunately lost.

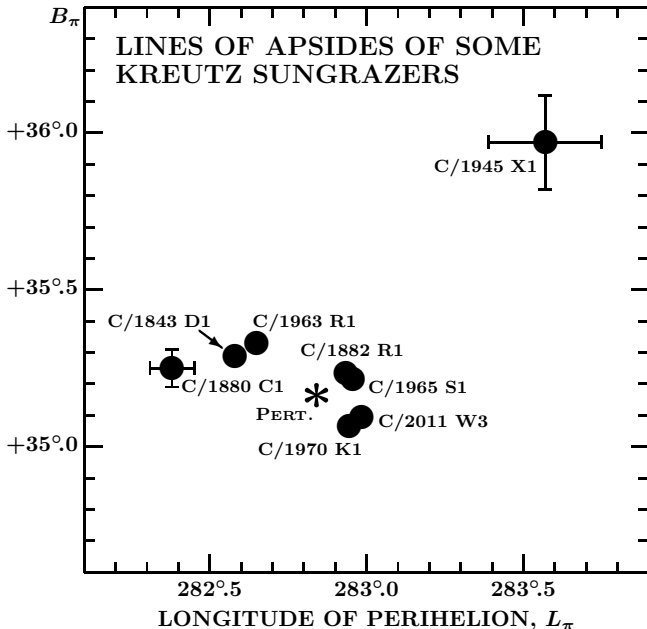


Figure 1. Line of apsides for seven bright Kreutz sungrazers and C/1945 X1. The plot of the perihelion longitude L_π against perihelion latitude B_π shows that C/1945 X1, represented by Marsden's cataloged gravitational orbit, deviates significantly from the cluster of the bright sungrazers, whose lines of apsides are closely aligned. The asterisk marked PERT. is the apsidal-line position for C/1945 X1 on the assumption that the comet is a fragment of a common parent with C/1882 R1, the difference being due entirely to the indirect planetary perturbations. For six comets the errors of the coordinates L_π , B_π are smaller than the size of the symbols; the estimated errors for C/1880 C1 and C/1945 X1 are depicted.

tities under (ii) and (iii), which depend on the perturbations by the planets, Jupiter in particular. We examine these perturbation effects next.

5. INDIRECT PERTURBATIONS BY THE PLANETS

Because of the nature of their orbits, the Kreutz comets cannot experience a close approach to the planets, including Jupiter. Nevertheless, the sungrazers' orbits are subjected to indirect planetary perturbations over the entire revolution about the Sun and, as a result, show limited variations.

Addressing this problem in some detail, Marsden (1967) began his investigation of the effects of indirect perturbations on a fragment, separating from its sungrazing parent at perihelion, by integrating the fragment's motion over the orbital period to the time t_π of next perihelion. First, he considered only Jupiter in a circular orbit in the plane of the ecliptic. He applied the equations for the variation of arbitrary constants and found that in this simplified scenario the fragment's orbital elements — the argument of perihelion ω , the longitude of the ascending node Ω , the inclination i , and the perihelion distance q — at time t_π depend on Jupiter's ecliptical longitude at this same time, $\Lambda_J(t_\pi)$, as follows:

$$\begin{aligned}\omega(\Lambda_J) &= \omega_0 + X_\omega \sin(\Lambda_J + \Lambda_0), \\ \Omega(\Lambda_J) &= \Omega_0 + X_\Omega \sin(\Lambda_J + \Lambda_0), \\ i(\Lambda_J) &= i_0 + X_i \sin(\Lambda_J + \Lambda_0), \\ q(\Lambda_J) &= q_0 - X_q \sin(\Lambda_J + \Lambda_0 - 90^\circ) \\ &= q_0 + X_q \cos(\Lambda_J + \Lambda_0),\end{aligned}\quad (1)$$

where ω_0, \dots, q_0 are constant terms, X_ω, \dots, X_q are amplitudes (all taken as positive numbers), and Λ_0 is a constant phase shift. Because of Jupiter's nonzero orbital eccentricity and the deviation of its orbital plane from the plane of the ecliptic, and also because of the indirect perturbations by the other planets, the quasi-periodic variations of the sungrazers' orbital elements are more complex. Marsden indicated that when only Jupiter's perturbations were accounted for, the amplitudes amounted to approximately $X_\omega = 1^\circ.1$, $X_\Omega = 1^\circ.4$, $X_i = 0^\circ.3$, and $X_q = 0.00039 \text{ AU} = 0.084 R_\odot$. Marsden further pointed out that his numerical integrations, which took into account the perturbations by the planets Jupiter to Neptune and by Pluto, resulted in expressions similar to Equation (1), with the amplitudes equal, respectively, to $1^\circ.6$, $2^\circ.1$, $0^\circ.4$, and $0.00046 \text{ AU} (= 0.099 R_\odot)$.

Since the longitude and latitude of perihelion, L_π and B_π , are related to the three angular elements by

$$\begin{aligned}\tan(L_\pi - \Omega) &= \tan \omega \cos i, \\ \sin B_\pi &= \sin \omega \sin i,\end{aligned}\quad (2)$$

the variation of the line of apsides is described, to a first approximation, by:

$$\begin{aligned}L_\pi(\Lambda_J) &= L_0 + X_L \sin(\Lambda_J + \Lambda_0), \\ B_\pi(\Lambda_J) &= B_0 + X_B \sin(\Lambda_J + \Lambda_0),\end{aligned}\quad (3)$$

where

$$\begin{aligned}X_L &= X_\Omega + (X_\omega \cos i_0 - X_i \cos \omega_0 \sin B_0) \sec^2 B_0, \\ X_B &= (X_\omega \cot \omega_0 + X_i \cot i_0) \tan B_0.\end{aligned}\quad (4)$$

Marsden noticed that the line of apsides is scarcely af-

ected by the indirect perturbations. To get a more profound insight into their influence on the orbital motion of C/1945 X1, we first integrated the orbit of its major presumed sibling, C/1882 R1 (see Table 1 of Sekanina & Chodas 2004),⁶ back in time to the 1106 perihelion. Next we varied the eccentricity incrementally and ran a set of orbits, obtained in this fashion, forward in time. Using the JPL DE405 ephemeris, we accounted for the perturbations by all eight planets, by Pluto, and by the three most massive asteroids, as well as for the relativistic effect. The increments were adjusted stepwise so that the perihelion times ranged between 1939 August 2 and 1951 August 29 at nearly constant intervals of about 100 days each; the length of the covered time period slightly exceeded Jupiter's orbital period. Checks showed that the relative errors accumulated over an integration period of $\sim 1600 \text{ yr}$ did not exceed $\sim 10^{-10}$ in the comet's position vector and its velocity vector.

The integrated perturbations of the six orbital parameters, ω , Ω , i , L_π , B_π , and q , for this period of sungrazers' arrival to perihelion are presented in Figure 2 as a function of Jupiter's longitude Λ_J at the perihelion times, t_π . The variations are not periodic in that the values of the elements at $\Lambda_J = 0^\circ$ in 1939 and 1951 differ by $0^\circ.70$ in ω , by $0^\circ.59$ in Ω , by $0^\circ.12$ in i , by $0.068 R_\odot$ in q , by $0^\circ.044$ in L_π , and by $0^\circ.012$ in B_π . From Figure 2 it follows that the variations for the last four parameters are reasonably well approximated by the thick sine curve, while those for ω and Ω are seen to deviate quite significantly, especially in the range of Jupiter's longitudes from 30° to 150° . For at least these two elements the scenario based on Jupiter in a circular orbit in the plane of the ecliptic is clearly inadequate.

The perturbation variations in the perihelion longitude L_π are a problem. Equation (3) suggests that the curve should be in phase with the variations in the argument of perihelion, the longitude of the ascending node, and the inclination, but Figure 2 demonstrates that it is not. Closer inspection shows that the reason for this discrepancy is the fact that the predicted amplitude given by Equation (3) is very close to zero (or, in fact, slightly negative) and that the actual variations in L_π in Figure 2 are determined by the second order terms that have been neglected in Equation (3). For the perihelion latitude B_π this is not the case and its variations are indeed in phase with ω , Ω , and i .

The numerical integration shows that the net amplitudes of the orbital parameters amount to $1^\circ.52$ in ω , $1^\circ.86$ in Ω , $0^\circ.39$ in i , $0^\circ.11$ in L_π (which at a latitude of $\sim 35^\circ$ represents an arc of $0^\circ.09$), $0^\circ.07$ in B_π , and 0.00051 AU or $0.110 R_\odot$ in q . These are typically within about 10% of the amplitudes given by Marsden for the four elements from Equation (1) above. The overall amplitude for the line of apsides is $0^\circ.11$, so that the range, $0^\circ.22$, is generally consistent with the apsidal difference of $0^\circ.30$ between C/1882 R1 and C/1843 D1 accumulated over a span of two orbital periods (or about 15–17 centuries), suggested for the age of the Kreutz system by Sekanina & Chodas (2004, 2007).

⁶ This presumption is based both on Marsden's (1967, 1989) and Sekanina & Chodas' (2004) conclusions and on the results of our own experimentation with the orbit of C/1945 X1, which showed that it was much easier to align its apsidal orientation with that of C/1882 R1 than C/1843 D1, the other potential major sibling.

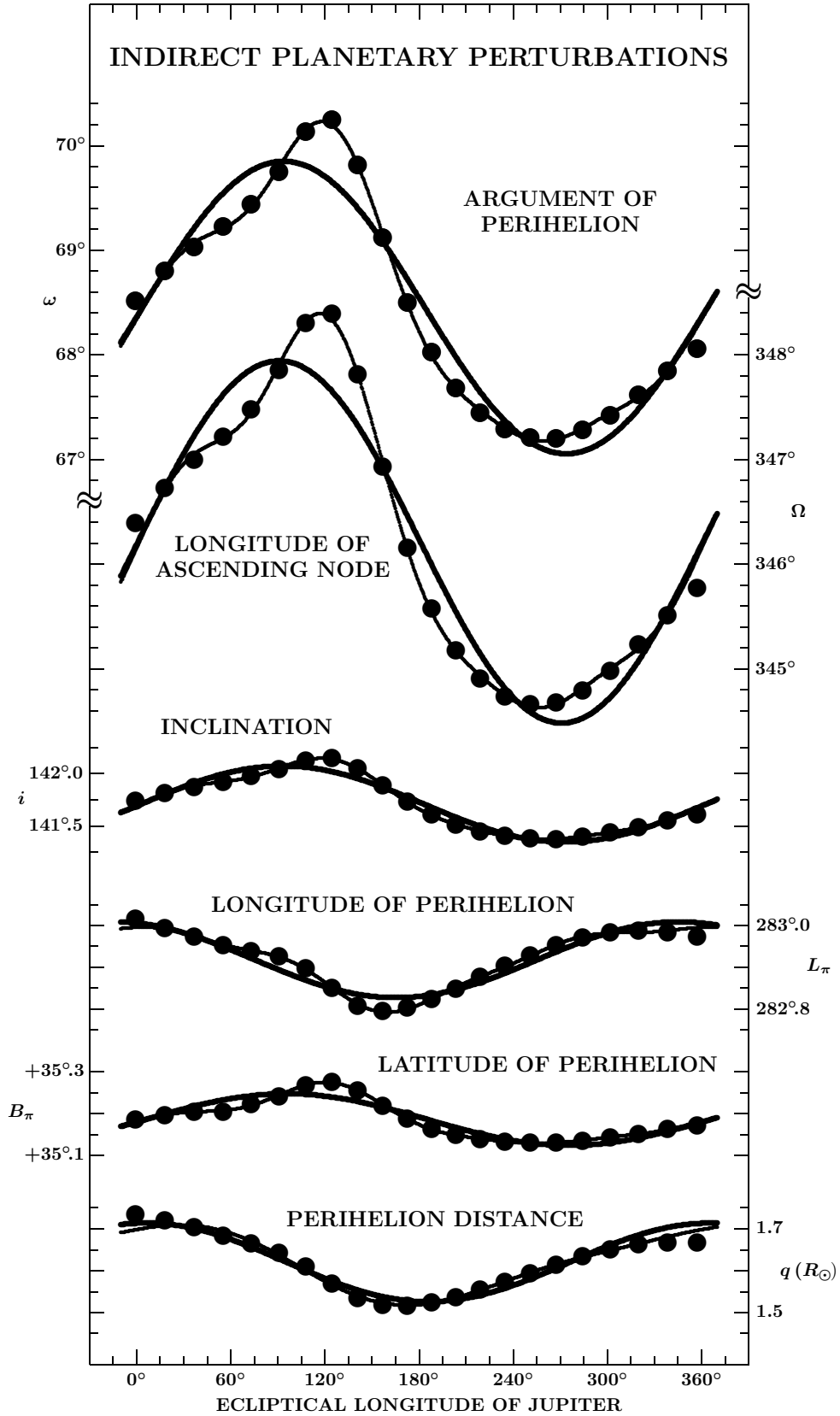


Figure 2. Plots, against the ecliptical longitude of Jupiter Λ_J at the time of a respective sungrazer's perihelion, of the argument of perihelion ω , the longitude of the ascending node Ω , the inclination i , the perihelion longitude L_π and latitude B_π (all equinox J2000), and the perihelion distance q of the siblings of comet C/1882 R1 separated at the 1106 perihelion, which returned to perihelion between 1939 August 2 and 1951 May 18. The sungrazer C/1945 X1 was at $\Lambda_J = 195^\circ.23$. The thick sine curves show the simple approximations of the type expressed by Equation (1), the thinner curves are the much better approximations by the N -harmonic Fourier polynomials ($N = 4$ for all but the last curve, for which $N = 2$; see Table 3). Note that the scales for L_π and B_π are four times wider than those for ω , Ω , and i .

Table 2
Cataloged Orbit of C/1945 X1 and Orbit of the Hybrid
(Equinox J2000).

Orbital element	C/1945 X1 (cataloged ^a)	Hybrid ^b (perturbed)
Perihelion time t_π (1945 TT)	Dec. 27.9652	Dec. 27.9801
Argument of perihelion ω	72°.0619	67°.8518
Longitude of ascending node Ω	351°.2006	345°.3759
Orbit inclination i	141°.8734	141°.5608
Perihelion distance q $\left\{ \begin{array}{l} \text{(AU)} \\ \text{(} R_\odot \text{)} \end{array} \right.$	0.007516 1.6147	0.007123 1.5302
Orbit eccentricity	1.0	0.99992634
Semimajor axis (AU)	∞	96.7
Orbital period (yr)	∞	951
Longitude of perihelion L_π	283°.57	282°.84
Latitude of perihelion B_π	+35°.97	+35°.16
Osculation epoch (1945 TT)	(none)	Dec. 26.0

^a See Marsden & Williams (2008).

^b Orbit of C/1882 R1 integrated to perihelion time of C/1945 X1.

We now constrain the orbital properties of C/1945 X1 by its arrival time at perihelion, 1945 December 28.0 TT. The predicted orientation of the comet's line of apsides is determined by the ecliptical coordinates $L_\pi = 282^\circ.84$ and $B_\pi = +35^\circ.16$ (Equinox J2000), deviating from the orientation of the apsidal line of C/1882 R1 by $0^\circ.11$. The longitude of Jupiter at the time of the comet's perihelion is $\Lambda_J = 195^\circ.23$. In addition, the computations show that the comet's osculating semimajor axis should have been 96.7 AU and the orbital period 951 yr, longer than the actual time span since 1106. This orbital period is in excellent agreement with the value that Sekanina & Chodas (2004) obtained for this comet in their hierarchy model of the Kreutz system (see their Table 12).

To illustrate the influence of the indirect perturbations specifically on the orbit of C/1945 X1, we compare Marsden's (1967) cataloged parabolic orbit (cf. Marsden & Williams' 2008) with the orbit of what we call a *hybrid* — one that C/1882 R1 would have had, if it arrived at perihelion at the time C/1945 X1 did. The two orbits differ by several degrees in the argument of perihelion and the longitude of the ascending node, and by almost $0.1 R_\odot$ in the perihelion distance.

Returning now to Figure 2, one could think of the differences between the sequence of the points, computed by numerical integration of the orbits, and the thick sine curves that are intended to fit them, as deformations and, accordingly, employ the superposition principle to mitigate the discrepancies. The effects of the perturbations, even though *not* periodic on a scale of Jupiter's orbital period, can nonetheless be expressed as a combination of periodic variations in terms of an N -harmonic Fourier polynomial. Figure 2 shows the results of this fitting, with N not exceeding 4, as the lighter curves; obviously, the improvement over a simple sine curve is considerable. Thus, calling \mathfrak{R} any of the six parameters in Equations (1) and (3), we can write it in the form:

$$\begin{aligned} \mathfrak{R}(\Lambda_J) &= \mathfrak{R}_0 + \sum_{k=1}^N [a_{\mathfrak{R},k} \sin(k\Lambda_J) + b_{\mathfrak{R},k} \cos(k\Lambda_J)] \\ &= \mathfrak{R}_0 + \sum_{k=1}^N X_{\mathfrak{R},k} \sin(k\Lambda_J + \Lambda_{\mathfrak{R},k-1}), \end{aligned} \quad (5)$$

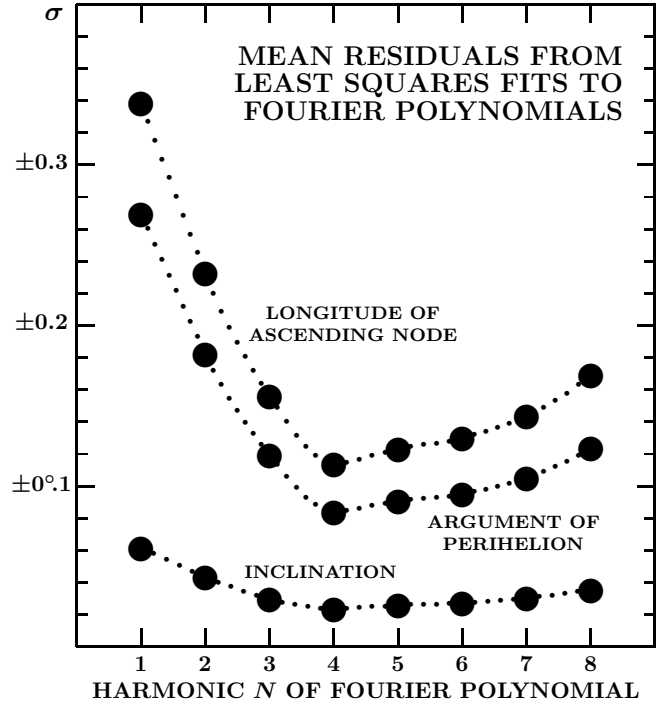


Figure 3. Mean residuals σ of the Fourier polynomials, fitted to the variations in the longitude of the ascending node, the argument of perihelion, and the inclination during Jupiter's orbital period 1939–1951, as a function of the polynomials' harmonic N . The minimum residual for all three orbital elements is reached at $N = 4$.

where

$$\begin{aligned} X_{\mathfrak{R},k} &= \sqrt{a_{\mathfrak{R},k}^2 + b_{\mathfrak{R},k}^2}, \\ \Lambda_{\mathfrak{R},k-1} &= \arctan\left(\frac{b_{\mathfrak{R},k}}{a_{\mathfrak{R},k}}\right). \end{aligned} \quad (6)$$

It is apparent that for $N = 1$, Equation (5) emulates Equations (1) and (3), with $\Lambda_{\mathfrak{R},0}$ being always equal to Λ_0 for $\mathfrak{R} = (\omega, \Omega, i, L_\pi, B_\pi)$ and $\Lambda_{\mathfrak{R},0} = \Lambda_0 + 90^\circ$ for $\mathfrak{R} = q$, and with $X_{\mathfrak{R},1} = X_{\mathfrak{R}}$ for any orbital parameter.

The coefficients $a_{\mathfrak{R},k}$ and $b_{\mathfrak{R},k}$ are computed by least squares from the values of $\mathfrak{R}(\Lambda_J)$ derived from the orbit integration runs as a function of Jupiter's longitude $\Lambda_J(t_\pi)$. The appropriate number of terms $N = N_{\min} > 1$ is determined by a minimum mean residual. As the number of Fourier coefficients in the equations of condition increases with N , the number of the degrees of freedom drops, thus causing the mean residual σ to increase. A byproduct is an increasing uncertainty of the Fourier coefficients in the (meaningless) polynomials with $N > N_{\min}$. As examples, the plots of the mean residuals for ω , Ω , and i vs N are displayed in Figure 3.

The Fourier solutions for the six orbital parameters in Figure 2 are listed in Table 3. For each parameter the first line provides the results of the approximate solution, fit A, by applying Equation (1) or (3). The second and following lines refer to the fitted Fourier polynomial, F_N . The mean residual σ is always followed by the constant term \mathfrak{R}_0 and by information on each harmonic k in the case of the N -harmonic Fourier polynomial: the harmonic amplitude $X_{\mathfrak{R},k}$ and phase $\Lambda_{\mathfrak{R},k-1}$.

We note that the amplitudes of all harmonics are determined with an error not exceeding $\pm 35\%$, but mostly

Table 3
Fourier Polynomials Fitting the Dependence of Indirect Planetary Perturbations of Orbital Elements of Kreutz Sungrazers in 1939–1951 on Ecliptical Longitude of Jupiter.

Orbital element	Fit ^a	Mean residual	Constant term ^b	Harmonic $k = 1, \dots, N$	Harmonic amplitude	Harmonic phase
Argument of perihelion, ω	A	$\pm 0^\circ 269$	$68^\circ 454 \pm 0^\circ 057$...	$1^\circ 397 \pm 0^\circ 083$	$356^\circ 2 \pm 3^\circ 3$
	F ₄	± 0.084	68.455 ± 0.018	1	1.386 ± 0.026	355.9 ± 1.0
				2	0.272 ± 0.026	202.1 ± 5.3
				3	0.183 ± 0.025	57.3 ± 8.0
				4	0.105 ± 0.025	319 ± 14
Longitude of ascending node, Ω	A	± 0.338	346.214 ± 0.072	...	1.731 ± 0.104	359.1 ± 3.3
	F ₄	± 0.113	346.216 ± 0.024	1	1.718 ± 0.035	358.8 ± 1.1
				2	0.338 ± 0.035	205.8 ± 5.8
				3	0.229 ± 0.034	59.0 ± 8.7
				4	0.134 ± 0.035	323 ± 15
Orbit inclination, i	A	± 0.061	141.709 ± 0.013	...	0.364 ± 0.019	357.0 ± 2.8
	F ₄	± 0.023	141.710 ± 0.005	1	0.361 ± 0.007	356.7 ± 1.1
				2	0.059 ± 0.007	198.6 ± 6.7
				3	0.042 ± 0.007	52.0 ± 9.6
				4	0.024 ± 0.007	320 ± 17
Longitude of perihelion, L_π	A	± 0.0202	282.9179 ± 0.0043	...	0.0968 ± 0.0060	104.6 ± 3.9
	F ₄	± 0.0087	282.9183 ± 0.0019	1	0.0906 ± 0.0026	104.1 ± 1.7
				2	0.0222 ± 0.0026	299.2 ± 6.9
				3	0.0077 ± 0.0027	143 ± 20
				4	0.0082 ± 0.0027	29 ± 18
Latitude of perihelion, B_π	A	± 0.0169	$+35.1860 \pm 0.0036$...	0.0616 ± 0.0052	354.4 ± 4.6
	F ₄	± 0.0030	$+35.1859 \pm 0.0006$	1	0.0608 ± 0.0009	353.8 ± 0.9
				2	0.0185 ± 0.0009	194.6 ± 2.7
				3	0.0111 ± 0.0009	66.3 ± 4.7
				4	0.0055 ± 0.0009	321.4 ± 9.3
Perihelion distance, q (R_\odot)	A	± 0.0156	1.6200 ± 0.0034	...	0.0987 ± 0.0048	84.0 ± 2.9
	F ₂	± 0.0132	1.6183 ± 0.0028	1	0.0905 ± 0.0039	83.2 ± 2.6
				2	0.0173 ± 0.0040	325 ± 13

^a A = approximation by Equation (1) or (3), based on the assumption of a single planet in circular orbit in the plane of the ecliptic; F_N = N-harmonic Fourier polynomial that provides the best fit (minimum mean residual).

^b Equinox J2000.

less than $\pm 25\%$. With one borderline exception the amplitudes decrease with increasing harmonic, as expected. The amplitude of the first harmonic is always only slightly smaller than the net amplitude derived directly from the results of numerical integration of the orbit. The phase angles of all harmonics for the argument of perihelion, the longitude of the ascending node, the inclination, and the latitude of perihelion are remarkably close to one another. The first harmonic for the perihelion distance is shifted, as expected, by almost exactly 90° relative to those of ω , Ω , i , and B_π . Only the longitude of perihelion L_π appears to be out of phase with any of the other orbital parameters.

The least-squares procedure also allows us to generalize Equation (5) thus:

$$\mathfrak{R}(\Lambda_J) = \mathfrak{R}_0 + \sum_{k=1}^N X_{\mathfrak{R},k} \sin(c_k \Lambda_J + \Lambda_{\mathfrak{R},k-1}), \quad (7)$$

where c_k 's are any positive numbers, not restricted to integers. This generalization offers us an opportunity to relate the coefficients c_k ($k > 1$) to the orbital periods of other planets, P_k , so that $c_k = P_J/P_k$. Without providing any details, we point out that our search for least-squares solutions of this type proved much less successful in fitting the quasi-periodic variations in the sungrazers' orbital elements than did the Fourier polynomials.

6. ORBITAL COMPUTATIONS BASED ON THE BOYDEN OBSERVATIONS FROM DECEMBER 11–15

If comet C/1945 X1 is closely related to C/1882 R1, the hybrid's orbit in Table 3 suggests that the line of apsides be described by $L_\pi = 282^\circ 84$ and $B_\pi = +35^\circ 16$ (Equinox J2000), as plotted in Figure 1 (marked PERT.), and that the osculating semimajor axis at perihelion be equal to $a = 96.7$ AU. Table 3 also shows that the osculating elements should differ from those of C/1882 R1 by $\sim 2^\circ$ in ω and Ω , by almost $0^\circ 5$ in i , and by more than $0.1 R_\odot$ in q . Below we investigate a range of orbital solutions, gravitational and nongravitational, offered by the observations made at Boyden on December 11–15.

As measured and reduced by Mowbray and listed for the equinox B1950 by Marsden (1989), the five astrometric positions are for the equinox J2000 presented in Table 4. Because on the first two nights the comet was imaged with the Cooke lens, while on the three remaining nights with the Metcalf refractor, we assign the positional data weights that are inversely proportional to the plate scales of the two instruments. Comparison of the observation times in column 2 of Table 4 with those in column 2 of Table 1 shows that the first ones are systematically too early by 0.00021 to 0.00022 day, or 18–19 s. The nature of the difference is unknown; it cannot come from a longitude discrepancy, because it is equivalent to

Table 4
Measured and Reduced Boyden Observations of Comet C/1945 X1 (Equinox J2000).

Ref. No.	Observation time		R.A.	Dec.	Assigned weight	Instrument employed	Plate number	From plate center	
	1945 (UT)							distance	P.A.
1	December 11.04687	15 ^h 13 ^m 24. ^s 42	−65°23′43. [″] 4	1.0	Cooke	AM 25201	11°94	124°4	
2	12.04691	15 43 21.25	−64 09 13.1	1.0	Cooke	AM 25206	2.89	68.0	
3	13.07189	16 11 04.21	−62 29 32.5	3.6	Metcalf	MF 34987	1.07	300.5	
4	14.07000 ^a	16 34 56.77	−60 33 16.5	3.6	Metcalf	MF 34991	1.16	302.6	
5	15.06885	16 55 41.67	−58 22 47.2	3.6	Metcalf	MF 34994	0.95	285.7	

^a Position reconstructed by Marsden for an arbitrarily chosen time on this date (see footnote in Section 4).

a distance of as much as ~ 500 meters. The UT times in Table 1, determined from the sidereal times of the beginning and end of the exposures, are in fact UT1 times and have independently been checked; they never left an unexplained difference of more than ~ 1 s. Nevertheless, for the sake of comparison with Marsden’s (1967, 1989) results, we retain for this exercise his UT times.

6.1. Gravitational Solutions

Since the observed orbital arc is too short to reliably compute the eccentricity, it needs to be determined from other considerations. As already mentioned above, the constraint is here provided by adopting the semimajor axis of the hybrid’s osculating orbit, 96.7 AU at the epoch of 1945 December 26.0 TT, for all solutions that follow. We begin with a gravitational orbit to fit all five astrometric positions in Table 4.

Deriving orbits B and C and comparing them with orbit A, Marsden (1989) demonstrated that elliptical solutions fitted the five observations of C/1945 X1 much better than a parabolic approximation. Yet, neither orbit, B or C, provides a satisfactory fit. One possible contributor to this problem could be the constraint introduced to satisfy the prescribed direction of the line of apsides (for which Marsden took $L_\pi = 282^\circ.7$, $B_\pi = +35^\circ.2$ after conversion to Equinox J2000), the same issue that we encountered with the dwarf sungrazers of the Kreutz system (Paper 1; see also Section 1).

Comparison of orbit C, the more realistic of the two sets in terms of the comet’s orbital period, with our optimum gravitational fit to the five observations is presented in Table 5. Marsden’s (1989) residuals from orbit C in this table have a tendency to become more positive toward both ends of the observed arc in right ascension and to get more negative with time in declination. We tried to emulate the residuals from orbit C, employing the set of truncated elements in Marsden’s (1989) Table V, but succeeded to achieve this within about $4''$ only in declination. Although we allowed for the rounding off of the perihelion time, the residuals in right ascension came out systematically more negative by about $12''$ and all except the last one were negative. This effect is due apparently to the elements’ truncation.

The residuals from our *Best Fit* solution, although clearly better than those from orbit C, are not quite satisfactory either, suggesting that the first observation may be inferior. That should not be surprising, considering that the comet was rather far from the plate center on this discovery exposure (Section 3). Unfortunately, the line of apsides deviates from the proper direction by

$0^\circ.571$, which is unacceptably large. Although the individual angular elements of the *Best Fit* solution are burdened with errors of up to several tenths of a degree, the correlation among them draws the uncertainty in the orientation of the line of apsides down to only hundredths of a degree.

Next, we compare Marsden’s (1989) orbit D with the hybrid’s orbit from Table 2. As with orbit C, we first tested whether the low-precision orbit D from Marsden’s Table V is able to reproduce the residuals in his Table VI. Since this exercise did not meet with success, we decided to reconstruct the high-precision version of orbit D, not published by Marsden, by subtracting the residuals in his Table VI from the observed astrometric positions, retaining his constraint on the reciprocal semimajor axis (0.01016 AU^{-1}). This approach was successful; the resulting orbit D is shown in Table 6 to be exceedingly similar to the hybrid’s orbit, the two sets of elements differing mostly in the fourth or higher significant digit. In particular, we note that the lines of apsides agree to bet-

Table 5
Marsden’s (1989) Orbit C and Our Optimum Gravitational Solution to Fit All Five Boyden Observations of C/1945 X1 (Equinox J2000).

Orbital element	Orbit C	<i>Best Fit</i>		
Perihelion time t_π (1945 TT)	Dec. 27.976	Dec. 27.982		
Argument of perihelion ω	68°10	70°99		
Longitude of ascending node Ω	345°54	349°50		
Orbit inclination i	141°60	141°91		
Perihelion distance q $\left\{ \begin{array}{l} (\text{AU}) \\ (R_\odot) \end{array} \right.$	0.00699 1.502	0.007244 1.556		
Orbit eccentricity	0.99993010	0.99992506		
Semimajor axis (AU)	100	96.67		
Orbital period (yr)	1000	950.5		
Longitude of perihelion L_π	282°70	283°14		
Latitude of perihelion B_π	+35°20	+35°68		
Osculation epoch 1945 (TT)	(none)	Dec. 11.0		
Mean residual ^a	$\pm 11''.95$	$\pm 6''.17$		
Distribution of Residuals ^a , $O - C$				
Time of observation 1945 (UT)	Orbit C		<i>Best Fit</i>	
	R.A.	Dec.	R.A.	Dec.
Dec. 11.04687	+5'6	+22'4	+13'2	+8'0
12.04691	+6.1	+5.3	+6.1	+2.5
13.07189	−14.8	−11.8	−6.6	−5.6
14.07000	+10.3	−1.9	+7.8	+8.0
15.06885	+15.6	−10.9	−2.7	−3.2

^a From unweighted observations for orbit C, weighted for *Best Fit*.

Table 6

Marsden’s (1989) Orbit D and Hybrid’s Orbit (Equinox J2000).

Orbital element	Orbit D	Hybrid’s orbit
Perihelion time t_π (1945 TT)	Dec. 27.9798 ^a	Dec. 27.9801
Argument of perihelion ω	67°.8356	67°.8514
Longitude of ascending node Ω	345°.3571	345°.3753
Orbit inclination i	141°.5553	141°.5607
Perihelion distance q $\begin{cases} (\text{AU}) \\ (R_\odot) \end{cases}$	$\begin{cases} 0.007129 \\ 1.5315 \end{cases}$	$\begin{cases} 0.007123 \\ 1.5302 \end{cases}$
Orbit eccentricity	0.99992756	0.99992632
Semimajor axis (AU)	98.42	96.67
Orbital period (yr)	976.4	950.5
Longitude of perihelion ^b , L_π	282°.84	282°.84
Latitude of perihelion ^b , B_π	+35°.16	+35°.16
Osculation epoch 1945 (TT)	Dec. 11.0	Dec. 11.0
Mean residual ^c	$\begin{cases} \pm 7''.63 \text{ (M)} \\ \pm 8''.17 \text{ (SK)} \end{cases}$	$\pm 13''.75$

Distribution of Residuals ^c , $O-C$						
Time of observation 1945 (UT)	Orbit D (M)		Orbit D (SK)		Hybrid’s orbit	
	R.A.	Dec.	R.A.	Dec.	R.A.	Dec.
Dec. 11.04687	+10''.8	+5''.1	+12''.3	+6''.6	+26''.4	-6''.3
12.04691	-2.5	-2.8	-1.1	-1.1	+13.7	-12.1
13.07189	-15.2	-11.4	-14.0	-9.6	+1.2	-18.7
14.07000	+4.3	+5.6	+5.3	+7.6	+20.4	0.0
15.06885	+2.8	+2.5	+3.6	+4.5	+18.4	-1.8

^aTo fit weighted observations, $t_\pi = \text{Dec. 27.9800}$.^bThese ecliptical coordinates define the reference line of apsides.^cEntry (M) and columns 2–3 from unweighted observations; entry (SK) and columns 4–5 from weighted observations; residuals from hybrid’s orbit are from weighted observations.

ter than 0°.01. This correspondence is not fortuitous, as both sets of elements represent perturbed versions of the orbits of two comets observed 83 years apart, whose motions in space were virtually identical, as already pointed out by Marsden (1967): C/1882 R1, used by us to derive the hybrid’s orbit; and C/1965 S1, employed by Marsden (1989) to derive orbit D.

Table 6 also lists three sets of residuals: those left by orbit D from the unweighted observations, in columns 2 and 3 [taken from Marsden’s (1989) Table VI and marked M]; those left by orbit D from the weighted observations, as derived by us⁷ (marked SK), in columns 4 and 5; and those left by the hybrid’s orbit from the weighted observations, in columns 6 and 7.

Even though the residuals in Table 6 are fairly large, the ones left by orbit D are much better than the strongly systematic ones left by the hybrid’s orbit. From this comparison as well as from the difference in the mean residual we infer that the orbital evolution of comet C/1945 X1, as a fragment of its common parent with C/1882 R1 and C/1965 S1, was apparently more similar to the orbital evolution of the latter than the former. This is an important though tentative conclusion, consistent with the fragmentation hierarchy of the Kreutz system proposed by Sekanina & Chodas (2004). According to their evolutionary model, C/1882 R1, C/1965 S1, and the precursor to C/1945 X1 separated from their common parent, possibly X/1106 C1, at the same time, some 18 days

⁷ This fit required that the perihelion time be increased by 0.0002 day relative to the tabulated value; otherwise the residuals would be slightly greater.

after perihelion. Relative to C/1882 R1, the precursor moved in the same direction as, and with a velocity only about 20% lower than, C/1965 S1 (see also Sekanina & Chodas 2002). The subsequent separation of C/1945 X1 from its precursor around 1700 AD notwithstanding, the comet’s orbit in 1945 should indeed resemble the orbit of C/1965 S1 to a greater degree than that of C/1882 R1.

Since orbit D and the hybrid’s orbit are so very similar, yet the residuals they leave substantially differ, we tested whether this effect is due to the minor differences in the angular elements or the orbital dimensions. We replaced the semimajor axis 98.4 AU with 96.7 AU and noted that the residuals from orbit D in Table 6 did not change; the new orbit, D’, is now: $t_\pi = 1945$ December 27.9803 TT, $q = 0.007126 \text{ AU} = 1.5309 R_\odot$, $e = 0.99992630$, and for the equinox of J2000, $\omega = 67°.8377$, $\Omega = 345°.3558$, and $i = 141°.5570$. The residuals in Table 6 reflect thus entirely the differences of up to 0°.02 in the angular elements.

Before turning to nongravitational solutions, we take notice of a possibility that one of the five astrometric observations is inferior and should be discarded before computing any orbit. Accordingly, we are now going to search for solutions that could fit four observations. Such solutions will be referred to as $\mathcal{G}\{\mathfrak{S}\}$, where \mathcal{G} stands for gravitational and $\{\mathfrak{S}\}$ is a progression of reference numbers of the observations that such solutions are based on; these numbers are listed in column 1 of Table 4. The *Best Fit* solution presented in Table 5 can now be referred to as $\mathcal{G}\{1, 2, 3, 4, 5\}$. As already mentioned above, the discovery position may be inferior, so that one of the tested four-observation solutions is $\mathcal{G}\{2, 3, 4, 5\}$. The residuals from orbit D in Table 6 suggest that the third observation may be even worse than the first, raising interest in the solution $\mathcal{G}\{1, 2, 4, 5\}$. Finally, the derivation of the cataloged parabolic orbit implied that the fourth observation failed to fit that solution (Marsden 1967), hence a need to test $\mathcal{G}\{1, 2, 3, 5\}$. The results of all three of these solutions are presented in Table 7. No orbits are being computed based on three observations only, as these are regarded for our purposes as meaningless.

Since a semimajor axis a between 96.7 AU and 98.4 AU was shown to make no difference, the four-observation solutions below are subjected to the same constraint as the *Best Fit* solution in Table 5, namely, $a = 96.7 \text{ AU}$ at an osculation epoch of 1945 December 26.0 TT. The solutions listed in Table 7 differ from one another considerably. The orbits $\mathcal{G}\{2, 3, 4, 5\}$ and $\mathcal{G}\{1, 2, 3, 5\}$ are both unacceptable on account of their large offsets from the reference apsidal direction (given by the hybrid’s orbit and Marsden’s orbit D). The set $\mathcal{G}\{2, 3, 4, 5\}$ is in addition handicapped by the very large residuals left by the December 12 observation. Even cursory inspection shows that the orbit $\mathcal{G}\{1, 2, 4, 5\}$ is by far the most promising of the three, implying that it is the December 13 observation that is inferior. The offset from the reference line of apsides, slightly less than 0°.1, is reasonably low though not completely satisfactory. It is somewhat surprising that the apparently inferior astrometric position is one of those taken with the Metcalf refractor. We would expect that the discarded data point should be one of the first two observations, made with the Cooke camera. Under the circumstances, the solution $\mathcal{G}\{1, 2, 4, 5\}$ can at best be regarded as marginally acceptable to approximate the orbital motion of C/1945 X1.

Table 7
Comparison of Three Gravitational Solutions Based on
Four Observations of C/1945 X1 (Equinox J2000).

Orbital element	$\mathcal{G}\{2, 3, 4, 5\}$	$\mathcal{G}\{1, 2, 4, 5\}$	$\mathcal{G}\{1, 2, 3, 5\}$
Perihelion time t_π (1945 TT)	Dec. 27.986	Dec. 27.979	Dec. 27.983
Argument of perihelion ω	65°.98	67°.43	74°.00
Longitude of ascending node Ω	342°.84	344°.82	353°.52
Orbit inclination i	141°.37	141°.50	142°.07
Perihelion distance q $\left\{ \begin{array}{l} \text{(AU)} \\ \text{(}R_\odot\text{)} \end{array} \right.$	0.007004 1.505	0.007120 1.530	0.007415 1.593
Orbit eccentricity	0.99992755	0.99992635	0.99992329
Longitude of perihelion L_π	282°.54	282°.80	283°.49
Latitude of perihelion B_π	+34°.77	+35°.09	+36°.22
Reference apsidal line's offset ^a	0°.462	0°.078	1°.184
Osculation epoch 1945 (TT)	Dec. 11.0	Dec. 11.0	Dec. 11.0
Mean residual (weighted)	±5''11	±1''79	±1''06

Distribution of Residuals ^b , $O - C$						
Time of observation 1945 (UT)	$\mathcal{G}\{2, 3, 4, 5\}$		$\mathcal{G}\{1, 2, 4, 5\}$		$\mathcal{G}\{1, 2, 3, 5\}$	
	R.A.	Dec.	R.A.	Dec.	R.A.	Dec.
Dec. 11.04687	+5''3	+1''1	-3''3	+3''3
12.04691	+25''2	+12''0	-8.2	-7.4	+4.9	+2.7
13.07189	-5.1	-4.3	+0.1	-0.8
14.07000	+4.3	+5.5	+0.1	+1.3
15.06885	-1.1	-2.3	+0.1	-0.8	-0.2	+0.3

^aReference line of apsides is defined by the hybrid's L_π and B_π .

^bFrom weighted observations.

In any case, it is worth examining whether any meaningful refinement of the orbit, an apsidal line in particular, can be achieved by incorporating a nongravitational acceleration, which, if comparable to those affecting the motions of the dwarf sungrazers, might be detectable over a span of four days. Besides, such alternative solutions should prove beneficial to estimating a range of uncertainties in the comet's orbital motion (Section 7).

6.2. Standard Nongravitational Solutions

In order to find out whether there is evidence for nongravitational effects in the motion of comet C/1945 X1 in the meager set of astrometric data available, we begin with a standard formalism of Marsden et al. (1973), based on a water-ice sublimation model. The erosion-driven nongravitational accelerations in the three cardinal directions, i.e., in the radial (away from the Sun), \mathbf{R} , transverse, \mathbf{T} , and normal, \mathbf{N} , directions of a right-handed \mathbf{RTN} coordinate system that is referred to the comet's orbital plane, are in this formalism expressed by

$$\begin{bmatrix} a_{\mathbf{R}}(r) \\ a_{\mathbf{T}}(r) \\ a_{\mathbf{N}}(r) \end{bmatrix} = \begin{bmatrix} A_1 \\ A_2 \\ A_3 \end{bmatrix} \cdot g_{\text{std}}(r), \quad (8)$$

where $g_{\text{std}}(r)$ is the standard law employed by Marsden et al. (1973), approximating the sublimation rate of water ice from an isothermal spherical nucleus and normalized so that $g_{\text{std}}(1 \text{ AU}) = 1$,

$$g_{\text{std}}(r) = \alpha \left(\frac{r}{r_0} \right)^{-m} \left[1 + \left(\frac{r}{r_0} \right)^n \right]^{-k}. \quad (9)$$

Here $m=2.15$, $n=5.093$, $nk=23.5$, a scaling distance $r_0=2.808 \text{ AU}$, and a normalization constant $\alpha=0.1113$.

The parameters A_1 , A_2 , A_3 are, respectively, the radial, transverse, and normal components of the nongravitational acceleration at 1 AU from the Sun; their units usually employed in orbital studies are $10^{-8} \text{ AU day}^{-2}$. Since the vector of the acceleration due to the generally sunward-directed sublimation points away from the Sun, physically meaningful values of A_1 should always be positive. The law (9) has over the past 40 years served admirably in countless orbit-determination applications to comets with perihelia typically several tenths of AU.

The numerical procedure that we apply next follows the method described in Paper 1. Briefly, since the direction of the line of apsides was found to be a function of the nongravitational acceleration, a minimum offset from the reference, or nominal, apsidal line (defined here by L_π and B_π for the hybrid's orbit or orbit D; see Table 6) serves as the constraint that determines the nongravitational acceleration's most probable magnitude.

Similarly to our notation for the gravitational runs, we refer to these nongravitational solutions by $\mathcal{N}_{\text{std}}^{(\infty)}\{\mathfrak{S}\}$, where $\{\mathfrak{S}\}$ is again a progression of reference numbers of the employed observations from Table 4, while $\mathcal{N}_{\text{std}}^{(\infty)}$ denotes, on the one hand, Marsden et al.'s (1973) formalism of accounting for the nongravitational effect, with the standard law (9) describing the variations with heliocentric distance; and, on the other hand, one of the two versions applied: either solving for the radial component of the acceleration with the parameter A_1 when $\mathbf{X} = \mathbf{R}$; or for the normal component with A_3 when $\mathbf{X} = \mathbf{N}$. Whenever we attempted to solve for both components, the run aborted. We recall that the radial component ($A_1 > 0$) dominates the magnitude of the nongravitational acceleration in the motions of the cataloged comets in nearly-parabolic orbits (Marsden & Williams 2008), while the

Table 8

Comparison of the Nongravitational Parameters and Test Results for Eight Orbital Solutions Based on Marsden et al.'s formalism.

Nongravitational solution	Parameter ^a A_1 or A_3	Apsidal-line ^b offset	Mean residual (weighted)
$\mathcal{N}_{\text{std}}^{(\mathbf{R})}\{1, 2, 3, 4, 5\}$	-0.82 ± 0.17	0°116	$\pm 6''.42$
$\mathcal{N}_{\text{std}}^{(\mathbf{R})}\{2, 3, 4, 5\}$	$+0.67 \pm 0.18$	0.118	± 5.05
$\mathcal{N}_{\text{std}}^{(\mathbf{R})}\{1, 2, 4, 5\}$	$+0.113 \pm 0.019$	0.013	± 1.73
$\mathcal{N}_{\text{std}}^{(\mathbf{R})}\{1, 2, 3, 5\}$	-1.70 ± 0.40	0.270	± 3.03
$\mathcal{N}_{\text{std}}^{(\mathbf{N})}\{1, 2, 3, 4, 5\}$	-1.87 ± 0.23	0.073	± 6.68
$\mathcal{N}_{\text{std}}^{(\mathbf{N})}\{2, 3, 4, 5\}$	$+1.54 \pm 0.30$	0.085	± 4.88
$\mathcal{N}_{\text{std}}^{(\mathbf{N})}\{1, 2, 4, 5\}$	$+0.234 \pm 0.018$	0.006	± 1.72
$\mathcal{N}_{\text{std}}^{(\mathbf{N})}\{1, 2, 3, 5\}$	-4.18 ± 0.65	0.212	± 2.61

^a In units of 10^{-5} AU day⁻².

^b Offset from direction of the reference line of apsides (Table 6).

normal component (A_3) was found to contribute significantly to the magnitude of the acceleration that affects the motions of the dwarf Kreutz sungrazers (Paper 1).

Table 8 summarizes the most important results from the runs based on Marsden et al.'s (1973) standard formalism. Altogether we computed eight such solutions for four different observational sets $\{\mathfrak{S}\}$, the same ones as before: $\mathcal{N}_{\text{std}}^{(\mathbf{R})}\{1, 2, 3, 4, 5\}$, $\mathcal{N}_{\text{std}}^{(\mathbf{R})}\{2, 3, 4, 5\}$, $\mathcal{N}_{\text{std}}^{(\mathbf{R})}\{1, 2, 4, 5\}$, $\mathcal{N}_{\text{std}}^{(\mathbf{R})}\{1, 2, 3, 5\}$; and similarly with **N** instead of **R**. Both the **R** and the **N** versions of the $\mathcal{N}_{\text{std}}^{(\mathbf{X})}\{1, 2, 3, 4, 5\}$ and $\mathcal{N}_{\text{std}}^{(\mathbf{X})}\{1, 2, 3, 5\}$ runs are inferior to their respective gravitational solutions (Tables 5 and 7) in terms of the mean residual: $\pm 6''.42$ (**R**) and $\pm 6''.68$ (**N**) against $\pm 6''.17$ in the case of the $\{1, 2, 3, 4, 5\}$ solution; and $\pm 3''.03$ (**R**) and $\pm 2''.61$ (**N**) against $\pm 1''.06$ in the case of the $\{1, 2, 3, 5\}$ solution. In addition, for these two sets of solutions the **R**-version parameters A_1 come out to be negative and therefore physically meaningless.

Even though the set $\{2, 3, 4, 5\}$ avoids the misfortunes of the sets $\{1, 2, 3, 4, 5\}$ and $\{1, 2, 3, 5\}$, its offsets from the reference line of apsides fail to improve over the corresponding offsets from $\{1, 2, 3, 4, 5\}$; in addition, the residuals left by the December 12 observation are comparable to those from the equivalent gravitational solution (Table 7) and entirely unacceptable. In summary, the standard nongravitational solutions based on the set $\{1, 2, 4, 5\}$ are by far the best, in terms of both the offset from the reference apsidal line and the mean residual. Also, both A_1 and A_3 of the $\{1, 2, 4, 5\}$ solutions come out in Table 8 to be almost or just about one order of magnitude smaller than those of the poor solutions.

As the final comments we note that (i) relatively to the gravitational fit in Table 7, both nongravitational solutions based on the set $\{1, 2, 4, 5\}$ improve the mean residual only marginally (from $\pm 1''.79$ to $\pm 1''.72/1''.73$), but reduce the offset from the reference apsidal line considerably (from $0^\circ.078$ to $0^\circ.013/0^\circ.006$); (ii) both A_1 and A_3 appear to be fairly well determined (with the relative errors of ± 8 – 17%) and on the same order of magnitude, $\sim 10^{-6}$ AU day⁻², as the parameters of the normal component of the nongravitational acceleration of the dwarf sungrazers C/2009 L5 and C/2006 J9 in Table 4 of Pa-

per 1; and (iii) these parameters are one order of magnitude greater than the peak values of A_1 for the cataloged comets in nearly-parabolic orbits and at least two orders of magnitude greater than the typical values of A_1 for such comets (Marsden & Williams 2008). In summary, there is some — though, due to the limited data, not overwhelming — evidence that in terms of the nongravitational effects in its orbital motion, C/1945 X1 may share the properties of some dwarf Kreutz sungrazers.

6.3. Modified Nongravitational Solutions

The EXORB7 orbit-determination code employed by the second author allows one to vary arbitrarily all five parameters of the nongravitational law (9) — the exponents m , n , k , the scaling distance r_0 , and the normalization constant α . This option facilitates a more robust orbital experimentation, when the standard nongravitational model of Marsden et al. (1973) fails to provide satisfactory results. In Paper 1 we gained some experience with what we hereafter refer to as a *modified* nongravitational law $g_{\text{mod}}(r; r_0)$, which is given by Equation (9), but while the three exponents remain unchanged from the standard law, the scaling distance varies broadly, always entailing a change in α as well.

The physics behind this sublimation-law experimentation involves a parallelism between the scaling distance r_0 and the *snow line*, a boundary of the zone in vacuum (or near vacuum), beyond which it is cold enough for a volatile substance to exist only in the solid phase. Calibrated by water ice, for which in the isothermal model $r_0 \simeq 2.8$ AU, this distance depends in the first approximation on the effective latent heat of sublimation, L (in

Table 9
Orbital Solutions $\mathcal{N}_{\text{std}}^{(\mathbf{R})}\{1, 2, 4, 5\}$ and $\mathcal{N}_{\text{std}}^{(\mathbf{N})}\{1, 2, 4, 5\}$
(Equinox J2000).

Orbital element	$\mathcal{N}_{\text{std}}^{(\mathbf{R})}\{1, 2, 4, 5\}$	$\mathcal{N}_{\text{std}}^{(\mathbf{N})}\{1, 2, 4, 5\}$
Perihelion time t_π (1945 TT)	Dec. 27.97928	Dec. 27.97938
Argument of perihelion ω	$67^\circ.910$	$67^\circ.883$
Longitude of ascending node Ω	$345^\circ.437$	$345^\circ.412$
Orbit inclination i	$141^\circ.572$	$141^\circ.565$
Perihelion distance q $\left\{ \begin{array}{l} \text{(AU)} \\ \text{(} R_\odot \text{)} \end{array} \right.$	0.0071167 1.5287	0.0071250 1.5307
Orbit eccentricity	0.99992638	0.99992629
Longitude of perihelion L_π	$282^\circ.82$	$282^\circ.83$
Latitude of perihelion B_π	$+35^\circ.16$	$+35^\circ.16$
Reference apsidal-line offset	$0^\circ.0133$	$0^\circ.0060$
Parameter A_1 (10^{-5} AU day ⁻²)	$+0.113^a$
Parameter A_3 (10^{-5} AU day ⁻²)	$+0.234^b$
Osculation epoch 1945 (TT)	Dec. 11.0	Dec. 11.0
Mean residual (weighted)	$\pm 1''.73$	$\pm 1''.72$

Distribution of Residuals $O-C$

Time of observation 1945 (UT)	$\mathcal{N}_{\text{std}}^{(\mathbf{R})}\{1, 2, 4, 5\}$		$\mathcal{N}_{\text{std}}^{(\mathbf{N})}\{1, 2, 4, 5\}$	
	R.A.	Dec.	R.A.	Dec.
Dec. 11.04687	$+4''.9$	$+2''.0$	$+4''.9$	$+1''.6$
12.04691	-8.2	-7.3	-8.0	-7.2
14.07000	$+0.3$	$+1.0$	$+0.2$	$+1.1$
15.06885	-0.1	-0.6	0.0	-0.7

^aWith a mean error of $\pm 0.019 \times 10^{-5}$ AU day⁻² (Table 8).

^bWith a mean error of $\pm 0.018 \times 10^{-5}$ AU day⁻² (Table 8).

cal mol⁻¹), of the sublimating species:

$$r_0 \doteq \left(\frac{\text{const}}{L} \right)^2, \quad (10)$$

where r_0 is expressed in AU and the constant is equal to 19 100 AU^{1/2} cal mol⁻¹. Marsden et al. (1973) showed that in a plot of log (normalized sublimation rate) against log (heliocentric distance) the value of r_0 shifts the curve left or right along the axis of heliocentric distance r . Hence, by properly choosing r_0 , the erosion-driven non-gravitational effects in the orbital motion of any comet can approximately be expressed by a universal curve of log (normalized sublimation rate) against log(r/r_0).

Highly refractory materials, such as metals or silicates, can sublimate only very close to the Sun, so that their snow line and scaling distance are much smaller than 1 AU. For example, for forsterite, the Mg end-member of the olivine solid solution system, the latent heat of sublimation is 130 000 cal mol⁻¹ (Nagahara et al. 1994), so that its $r_0 \simeq 0.02$ AU.

In limiting cases the empirical equation (9) offers the following expressions for variations in the sublimation rates (equally applying to the modified and standard laws):

$$\begin{aligned} \lim_{x \rightarrow 0} g_{\text{mod}}(r; r_0) &\sim r^{-2.15}, \\ \lim_{x \rightarrow \infty} g_{\text{mod}}(r; r_0) &\sim r^{-25.65}. \end{aligned} \quad (11)$$

where $x = r/r_0$. The first limit approaches an extreme scenario in which all incident solar energy is spent on sublimation, while the second limit crudely approximates the other extreme, when the energy is spent entirely on heating the object (and increasing its thermal reradiation). The actual limiting expressions are r^{-2} for $r/r_0 \rightarrow 0$ and

$$\gamma_{\text{mod}}(r; r_0) \sim \exp\left(-\frac{L}{RT}\right) \quad \text{for } r/r_0 \rightarrow \infty, \quad (12)$$

where the sublimation heat L is related to r_0 by Equation (10), R is the gas constant, and T is the temperature at heliocentric distance r . The differences relative to (11) are due to the approximate nature of the law (9), which is responsible for a peculiar feature when applied to the orbital motion of C/1945 X1 (see below). To illustrate it, we begin by introducing a local slope ζ of a modified nongravitational law between r and $r + \Delta r$; similarly to (11), it is

$$\lim_{\Delta r \rightarrow 0} g_{\text{mod}}(r; r_0) \sim r^{-\zeta}, \quad (13)$$

where

$$\zeta(r; r_0) = -\frac{\partial \ln g_{\text{mod}}(r; r_0)}{\partial \ln(r/r_0)} = m + \frac{nk}{1 + (r/r_0)^{-n}}. \quad (14)$$

The limits on ζ are those given in (11). Since r_0 is nearly 3 AU in the standard law, the contribution to the integrated nongravitational effect from $r \gg r_0$ is always negligible and the exact shape of the standard nongravitational law at heliocentric distances $r \gg r_0$ is unimportant. However, when r_0 in a modified law is considerably smaller than that of the standard law, the power-law approximation to the exponential law for the sublimation

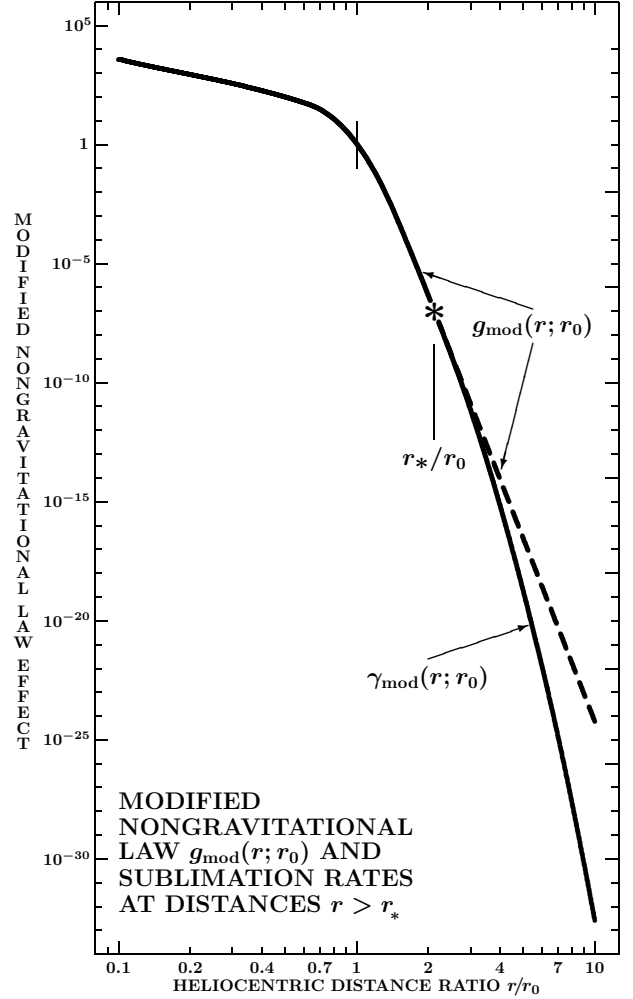


Figure 4. The nongravitational effects in the orbital motion of a comet derived from the modified law $g_{\text{mod}}(r; r_0)$ applicable to an arbitrary scaling distance r_0 . At heliocentric distances $r > r_*$ the law $\gamma_{\text{mod}}(r; r_0)$ matches the exponential variations in the sublimation rate better than $g_{\text{mod}}(r; r_0)$. The laws $g_{\text{mod}}(r; r_0)$ and $\gamma_{\text{mod}}(r; r_0)$ have equal logarithmic slopes at r_* . The slope ζ of $g_{\text{mod}}(r; r_0)$ at $r > r_*$ is practically constant.

rate beyond r_0 could play a major role for comets whose perihelion distances q are much greater than r_0 .

To find out at what heliocentric distance r_* does a modified law begin to deviate from the sublimation law $\gamma_{\text{mod}}(r; r_0)$, we first define the local slope ξ of $\gamma_{\text{mod}}(r; r_0)$ similarly to (14):

$$\xi(r; r_0) = -\frac{\partial \ln \gamma_{\text{mod}}(r; r_0)}{\partial \ln(r/r_0)} = \frac{L\sqrt{r}}{2RT_0} = \frac{L\sqrt{r_0}}{2RT_0} \sqrt{\frac{r}{r_0}}, \quad (15)$$

where $T(r) = T_0/\sqrt{r}$ at the heliocentric distances of extremely low sublimation rates; for the isothermal model, $T_0 = 278.3$ K. Since, from Equation (10), $L\sqrt{r_0}$ is a constant and $L\sqrt{r_0}/RT_0 = 34.54$, the point of deviation of the modified law $g_{\text{mod}}(r; r_0)$ from the exponential sublimation law, given by the condition of equal slopes, $\xi(r_*; r_0) = \zeta(r_*; r_0)$, determines r_* by comparing (14) with (15). After inserting the numerical values,

$$r_* = 2.12 r_0. \quad (16)$$

Less than a millionth part of the Sun’s incident energy at the distance r_* is spent on the sublimation.

Requiring that $g_{\text{mod}}(r_*; r_0) = \gamma_{\text{mod}}(r_*; r_0)$ and writing the exponential sublimation law in the form

$$\gamma_{\text{mod}}(r; r_0) = \beta \exp \left[34.54 \left(1 - \sqrt{\frac{r}{r_0}} \right) \right], \quad (17)$$

we have

$$\beta = 0.0267\alpha. \quad (18)$$

The relationship between $g_{\text{mod}}(r; r_0)$ and $\gamma_{\text{mod}}(r; r_0)$ is displayed in Figure 4. At present, the $\gamma_{\text{mod}}(r; r_0)$ law is not incorporated into the orbit-determination code that we employ, as in most cases it would make hardly any difference numerically. However, the approximation of $\gamma_{\text{mod}}(r; r_0)$ by $g_{\text{mod}}(r; r_0)$ at $r > r_*$ (i) prevents one from testing nongravitational laws with a variable exponent ζ at these heliocentric distances and (ii) yields identical results from all solutions based on the scaling distances r_0 that are by more than $2.12r_0$ smaller than the least heliocentric distance at which the comet is observed, as seen from Figure 4.

In Paper 1 we employed the modified-law paradigm to great advantage. We determined for all eight in-depth examined dwarf sungrazers that the astrometric positions were fitted better (and the offsets from the reference line of apsides came out to be smaller) when the nongravitational acceleration affecting their orbital motions was assumed to vary with heliocentric distance r much more steeply than prescribed by the standard law $g_{\text{std}}(r)$. The orbital motions of six out of the eight cases were fitted best with $r_0 < 0.13$ AU, which corresponds to $L \gtrsim 50\,000$ cal mol $^{-1}$, and for none of the eight was r_0 higher than ~ 2.1 AU. The heliocentric distances of the dwarf Kreutz sungrazers in Paper 1 varied between 0.037 and 0.068 AU (or between 8 and 15 R_{\odot}), so that these objects were considerably closer to the Sun than C/1945 X1 when under observation from Boyden.

For C/1945 X1, the modified-law nongravitational solutions with $r_0 \ll 0.2$ AU fit most satisfactorily the preferred set of four observations, $\{\mathfrak{S}_0\} = \{1, 2, 4, 5\}$. This match is better than that from the standard-law solutions listed in Table 9. We refer to these modified-law solutions as $\mathcal{N}_{\text{mod}}^{(\mathbf{X})}[r_0]\{\mathfrak{S}_0\}$, where \mathbf{X} has the same meaning as before and r_0 is in AU. Because the comet was not observed closer to the Sun than 0.6 AU, all these solutions are identical, as pointed out more generally under (ii) below Equation (18). We confirm this result by running solutions for r_0 equal to 0.01, 0.05, and 0.10 AU. We then select, as examples, the solutions $\mathcal{N}_{\text{mod}}^{(\mathbf{R})}[0.05]\{\mathfrak{S}_0\}$ and $\mathcal{N}_{\text{mod}}^{(\mathbf{N})}[0.05]\{\mathfrak{S}_0\}$ and present them in Table 10; relative to the results based on the standard law, the offsets from the reference line of apsides now dropped, respectively, from $0^\circ.013$ to $0^\circ.005$ and from $0^\circ.006$ to $0^\circ.003$, while the weighted mean residuals dropped, respectively, from $\pm 1''.73$ and $\pm 1''.72$ down to $\pm 1''.66$ in both \mathbf{R} and \mathbf{N} .

The nongravitational parameters A_1 and A_3 are now determined with relative errors of only ± 5 –7%. Their apparent discrepancy of nearly five orders of magnitude compared to those of the standard law is due entirely to the very different steepness of the two laws’ slopes. Since the comet was observed between 0.718 AU from the Sun (on December 11) and 0.598 AU from the Sun

Table 10
Orbital Solutions $\mathcal{N}_{\text{mod}}^{(\mathbf{R})}[0.05]\{\mathfrak{S}_0\}$ and $\mathcal{N}_{\text{mod}}^{(\mathbf{N})}[0.05]\{\mathfrak{S}_0\}$
(Equinox J2000).

Orbital element	$\mathcal{N}_{\text{mod}}^{(\mathbf{R})}[0.05]\{\mathfrak{S}_0\}$	$\mathcal{N}_{\text{mod}}^{(\mathbf{N})}[0.05]\{\mathfrak{S}_0\}$
Perihelion time t_π (1945 TT)	Dec. 27.97937	Dec. 27.97940
Argument of perihelion ω	$67^\circ.876$	$67^\circ.869$
Longitude of ascending node Ω	$345^\circ.403$	$345^\circ.397$
Orbit inclination i	$141^\circ.562$	$141^\circ.561$
Perihelion distance q $\left\{ \begin{array}{l} (\text{AU}) \\ (R_{\odot}) \end{array} \right.$	0.0071256 1.5308	0.0071279 1.5313
Orbit eccentricity	0.99992629	0.99992626
Longitude of perihelion L_π	$282^\circ.83$	$282^\circ.84$
Latitude of perihelion B_π	$+35^\circ.16$	$+35^\circ.16$
Reference apsidal-line offset	$0^\circ.0055$	$0^\circ.0034$
Parameter A_1 (10^{-10} AU day $^{-2}$)	$+0.307^a$
Parameter A_3 (10^{-10} AU day $^{-2}$)	$+0.877^b$
Osculation epoch 1945 (TT)	Dec. 11.0	Dec. 11.0
Mean residual (weighted)	$\pm 1''.66$	$\pm 1''.66$

Distribution of Residuals $O-C$

Time of observation 1945 (UT)	$\mathcal{N}_{\text{mod}}^{(\mathbf{R})}[0.05]\{\mathfrak{S}_0\}$		$\mathcal{N}_{\text{mod}}^{(\mathbf{N})}[0.05]\{\mathfrak{S}_0\}$	
	R.A.	Dec.	R.A.	Dec.
Dec. 11.04687	$+4''.7$	$+2''.0$	$+4''.8$	$+1''.7$
12.04691	-8.0	-6.9	-7.9	-6.9
14.07000	$+0.3$	$+0.9$	$+0.3$	$+1.0$
15.06885	-0.1	-0.5	0.0	-0.6

^aWith a mean error of $\pm 0.021 \times 10^{-10}$ AU day $^{-2}$.

^bWith a mean error of $\pm 0.046 \times 10^{-10}$ AU day $^{-2}$.

(on December 15), the magnitudes of the effective nongravitational accelerations need to be compared in this range of heliocentric distances, rather than at 1 AU from the Sun, to test whether the results from the standard law and the modified law are generally consistent. This test shows that the radial components from the two laws reach the same value, $+0.3 \times 10^{-5}$ AU day $^{-2}$, at $r = 0.639$ AU, while the normal components equally reach $+0.6 \times 10^{-5}$ AU day $^{-2}$ at $r = 0.648$ AU, in either case well inside the observed range of heliocentric distances. The comet’s favorable comparison with the dwarf sungrazers, mentioned in Section 6.2, is consistent with the results from the modified-law solutions: C/1945 X1 appears to be subjected to a nongravitational acceleration that is near the lower end of the range of accelerations typical for the dwarf sungrazers.

In summary, we obtain some evidence suggesting that (i) the nongravitational solutions fit the observations of C/1945 X1 better than the gravitational solutions; and (ii) a law with a very steep slope (of the type $\sim r^{-25}$) may be superior to the standard law. Over all, however, the promising performance of the modified law has not overturned our conclusion expressed at the end of Section 6.2 that the limited data sample does not make a conclusion about the existence of large nongravitational effects in the motion of C/1945 X1 sufficiently compelling. Every effort should be expended to improve the comet’s orbit by extending the observed arc with the help of additional images on Boyden patrol plates.

6.4. Astrometric and Orbital Accuracy

It may seem to be questionable to use the astrometric data of less than high quality for supporting the type of

Table 11
Geocentric Ephemeris for Comet C/1945 X1 from 1945 September 12 to 1946 January 30 (Equinox J2000).

Date TT	From solution $\mathcal{N}_{\text{mod}}^{(\text{N})}[0.05]\{\mathfrak{S}_0\}$				Phase angle	PA(RV)	App. magnitude		Differential ephemerides from solutions					
	R.A.	Dec.	Δ	r			r^{-4}	r^{-7}	$\mathcal{N}_{\text{std}}^{(\text{N})}\{\mathfrak{S}_0\}$	$\mathcal{G}\{\mathfrak{S}_0\}$	orbit D'			
1945 Sept. 12	7 ^h 39 ^m .0	-10°00'	2.860	2.466	20°1	258°5	15.7	19.7	-0.31	+2.5	-2.8	+117"	-0.25	+10.3
22	7 50.1	-11 48	2.592	2.310	22.7	263.5	15.2	19.0	-0.31	+2.7	-2.8	+116	-0.26	+10.3
Oct. 2	8 01.6	-14 03	2.315	2.148	25.6	268.2	14.6	18.2	-0.32	+2.8	-2.9	+115	-0.27	+10.4
12	8 13.7	-16 54	2.031	1.980	28.8	272.8	14.0	17.3	-0.33	+3.0	-3.0	+113	-0.29	+10.4
22	8 27.0	-20 36	1.744	1.804	32.5	277.2	13.3	16.3	-0.34	+3.2	-3.1	+110	-0.31	+10.4
Nov. 1	8 42.3	-25 33	1.458	1.619	37.2	281.5	12.4	15.1	-0.35	+3.4	-3.2	+107	-0.35	+10.3
11	9 02.4	-32 30	1.180	1.423	43.5	285.4	11.4	13.6	-0.38	+3.5	-3.3	+94	-0.40	+10.0
21	9 35.1	-42 48	0.922	1.213	53.0	286.9	10.2	11.9	-0.42	+3.2	-3.5	+71	-0.53	+8.9
Dec. 1	10 54.6	-57 49	0.713	0.982	69.1	277.1	8.7	9.7	-0.46	+1.5	-3.3	+30	-0.90	+5.6
6	12 34.0	-65 04	0.645	0.855	80.7	256.5	7.9	8.5	-0.36	+0.1	-2.1	+8	-1.22	+1.7
11	15 11.8	-65 27	0.617	0.719	94.6	219.8	7.0	7.0	-0.03	+0.1	-0.1	+1	-0.97	-3.4
16	17 12.4	-56 11	0.640	0.569	108.9	189.8	6.1	5.3	+0.04	+1.7	-0.3	-4	-0.39	-5.9
1946 Jan. 5	18 32.1	-42 17	0.662	0.434	126.4	201.3	5.0	3.4	+0.99	-8.7	+9.8	+204	+1.10	+19.9
10	19 14.6	-55 37	0.566	0.601	114.8	184.7	6.1	5.5	+2.02	-7.4	+22.1	+219	+2.12	+22.3
20	0 37.9	-69 21	0.525	0.882	84.7	104.0	7.6	8.2	+0.66	+17.4	+36.6	+508	+1.78	+44.0
30	3 32.8	-48 43	0.664	1.124	60.6	70.5	9.1	10.6	-1.47	+4.7	-2.8	+723	-0.87	+55.6

in-depth orbital analysis of C/1945 X1 that is described in the previous sections. With the observed arc of merely four days and the images taken with small cameras of poor spatial resolution and long exposures tracked at sidereal rates, the data may at first sight seem overexploited. However, the addressed objectives are not only to learn as much as possible about the orbital behavior of C/1945 X1 in the context of other Kreutz sungrazers, but, as illustrated in Table 11, also to provide a basis for constraining an ephemeris for the comet's motion both back and forward in time from the observed period, a capability that is amply put to use in our search for more images of the comet, as described in Section 7.

7. SEARCH FOR MORE DATA ON COMET C/1945 X1

The preceding sections demonstrate that, in spite of some evidence to the contrary, the current level of our knowledge of comet C/1945 X1 is less than sufficient for addressing the issue of whether or not this object was indeed a dwarf Kreutz sungrazer. It is essential that, where at all possible, existing information be rechecked, reanalyzed, and reinterpreted, and that a vigorous search for, and examination of, additional data be undertaken. All our efforts will be aided substantially by products of the Harvard College Observatory's DASCH Project, currently in progress, that we referred to in Section 3. As for the new data, our proposed work has three objectives: (i) to identify, astrometrically measure, and reduce any further images of the comet in the collection of digitized Boyden patrol plates (once they become available) with the aim to refine the orbit by extending the arc covered by observations as far back in time as possible; (ii) to constrain the comet's physical behavior by deriving magnitudes from all relevant digitized photographs and compare the comet's light curve with that of other sungrazers; and (iii) to search for and examine the comet's post-perihelion images taken at Boyden for any traces of the object or its debris, including the presence, appearance, and orientation of a headless tail, diagnostic of the object's fate near perihelion.

7.1. Search for Additional Images

Our extensive orbit examination in Section 6 allows us now to extrapolate, with a fair degree of confidence, the comet's motion way beyond the period of December 11–15 and to realistically estimate uncertainties of an ephemeris as a function of time. The nominal geocentric ephemeris of the comet for the period of time from 1945 September 12.0 TT to 1946 January 30.0 TT, presented in Table 11, is computed from the nongravitational solution $\mathcal{N}_{\text{mod}}^{(\text{N})}[0.05]\{\mathfrak{S}_0\}$ (whose elements and residuals are in Table 10), but the differential ephemerides, derived from the solution $\mathcal{N}_{\text{std}}^{(\text{N})}\{\mathfrak{S}_0\}$ (elements and residuals in Table 9), from the gravitational solution $\mathcal{G}\{\mathfrak{S}_0\}$ (Table 7), and from the orbit D' (see the text near Table 6), are also included for comparison. The two numbers listed in Table 11 for each of these three additional solutions are the corrections in right ascension and declination, respectively, that are to be added to the nominal coordinates in columns 2 and 3; note the different units used.

The first six columns of Table 11 are self-explanatory. The seventh column gives the position angle of the prolonged radius vector (direction away from the Sun), and the eighth and ninth columns include a predicted apparent magnitude on two assumptions for the brightness variations: as an inverse fourth and inverse seventh power of heliocentric distance, with no phase effect. Both versions were normalized to the comet's reported magnitude 7 at discovery on December 11, which predicts a magnitude of 9.5 at 1 AU from both the Sun and the Earth for the inverse fourth-power law and 10.6 for the inverse seventh-power law (see Section 7.2).

We find the agreement among the ephemerides based on the orbit D' and the two nongravitational solutions quite remarkable. On the other hand, the ephemeris from the gravitational solution based on the same observations as the two nongravitational orbits is very disappointing, differing from the other three by as much as 0°.2 over the period of 4.5 months. We note that the three consistent ephemerides come from the orbital sets that imply that

Table 12
Additional Boyden Plates with Possible Images of Comet C/1945 X1.

Plate number ^a	UT time at mid-exposure	Plate center ^b		Exp. time (min)	Logbook reference	Comet's position (absolute and relative) ^{b,c}						Observer ^d
		R.A.	Dec.			R.A.	Dec.	Plate	Dist.	P.A.	Edge	
RB 14049	1945 Sept. 19.11997	8 ^h 04 ^m 6	−15°17′	60	rb10_148	7 ^h 46 ^m 9	−11°13′	ON	5°91	312°6	6°85	Bl(?)
AM 25110	Oct. 10.07683	7 04.5	−15 09	85	am45b_0144	8 11.4	−16 18	ON	16.11	96.3	1.18	du Toit
RB 14086	17.07399	8 04.0	−30 17	120	rb10_132	8 20.3	−18 39	ON	12.20	18.5	2.33	J(?)
AM 25132	27.06607	9 03.5	−45 24	60	am45b_0148	8 34.4	−22 55	OFF	23.25	342.8	0.71	Bl(?)
AM 25145	Nov. 5.05881	9 04.2	−30 24	90	am45b_0150	8 49.7	−28 04	ON	3.93	305.4	13.99	Bester
AM 25150	12.06740	10 04.0	−45 29	80	am45b_0152	9 05.1	−33 25	ON	16.54	311.8	4.87	J(?)
RB 14121	13.03559	8 03.2	−45 17	120	rb10_138	9 07.6	−34 16	OFF	16.51	53.8	2.12	Bl(?)
AM 25169	15.06371	10 33.7	−60 31	85	am45b_0154	9 13.4	−36 11	OFF	27.50	323.1	0.50	J(?)
AM 25187	Dec. 7.04693	11 04.6	−45 32	90	am45b_0156	13 04.0	−65 58	OFF	25.94	152.4	1.49	du Toit
AM 25190	8.01580	10 33.7	−60 31	90	am45b_0156	13 34.2	−66 28	ON	20.50	126.1	0.63	J(?)
AM 25208	14.03336	16 40.9	−70 12	40	am45b_0158	16 34.1	−60 38	ON	9.60	355.0	11.94	J(?)
AM 25231 ^e	1946 Jan. 5.04600	12 05.2	−70 33	90	am45b_0162	18 32.4	−42 24	OFF	52.65	112.7	31.37	Bl(?)
RB 14183 ^e	6.04985	12 05.2	−60 33	115	rb10_148	18 38.1	−44 57	OFF	55.57	121.9	35.99	Bl(?)
RB 14184 ^f	8.07729	17 17.5	−47 19	40	rb10_148	18 53.5	−50 19	OFF	16.02	109.7	3.88	Bester
AM 25240	21.79113	0 05.1	−44 27	90	am45b_0164	1 36.3	−66 22	OFF	25.13	158.5	1.89	Britz
AM 25241	21.84446	1 33.6	−59 29	60	am45b_0164	1 37.8	−66 15	ON	6.78	176.5	14.73	Britz
AM 25244	24.85635	5 25.4	−68 55	90	am45b_0164	2 40.0	−59 43	OFF	19.62	277.3	2.26	Bl(?)
AM 25260	30.85589	5 03.9	−29 52	90	am45b_0166	3 38.4	−47 05	ON	23.86	217.8	2.56	Bl(?)

^a AM plates taken with the Cooke lens (covering 34°48 in R.A. and 43°10 in Dec.); RB plates with the Ross-Fecker camera (22°32 by 27°90).
^b Equinox J2000.

^c Column *Plate* indicates whether or not the comet's predicted position is within the plate limits; columns *Dist.* and *P.A.* show the predicted position relative to the plate center; and in column *Edge* is the distance of the comet's image from the plate edge (either on or off the plate).

^d The identities of the observers whose abbreviations are Bl and J could not be determined, major efforts notwithstanding; see also Table 1.

^e This plate may show a segment of an early post-perihelion tail, if the comet still produced significant amounts of dust (see Figure 6 or 7).

^f This is the only deliberate attempt at detecting C/1945 X1 after perihelion; unfortunately, the searched position is incorrect (see Figure 5).

the line of apsides lies within 0°.01 of the reference value, while the $\mathcal{G}\{\mathfrak{S}_0\}$ set leaves an offset of nearly 0°.08.

To further appraise the magnitude of ephemeris uncertainties, we completed 200 Monte Carlo runs with pure gravitational solutions fitted to the $\{\mathfrak{S}_0\}$ set of observations, assuming, conservatively, measuring errors of up to $\pm 9''$ in the December 11–12 positions and up to $\pm 2''.5$ in the December 14–15 positions. The standard deviations from the 200 clones vary, in the 1945 September–November period, between 2'.4 and 3' in right ascension and between 1'.4 and 5' in declination; in the 1946 January period, the range is from 6' to nearly 20' in right ascension and from 8' to 31' in declination. On the average the offsets of the $\mathcal{G}\{\mathfrak{S}_0\}$ -based ephemeris in Table 11 amount to about 40% of these standard deviations. To sum it up, we believe that our nominal ephemeris is accurate, in a worst case scenario, to a few arcmin over the entire period of interest to us.

The next step is a search for all patrol plates whose fields cover (or could cover) the comet's ephemeris position. Ideally, the physical size of each plate and its scale provide the angular distance from the center to an edge as a function of a position angle. It is in principle very easy to establish whether the comet's image is or is not located within the plate's limits. In reality, the problem is less straightforward because of a potentially significant error in the reported position of the plate center. Because of this uncertainty (much larger than in the ephemeris), the comet's predicted position may not be within the limits of a plate when it should, or vice versa. The search is further complicated by the comet's unknown brightness, the observing conditions (the sky transparency, the moon interference, the limiting magnitude, etc.), the ex-

posure time, and the distribution of field stars (needed for the astrometry), all of which determines whether the comet's image, even if present on the plate, can in fact be recognized, astrometrically measured and reduced, and photometrically evaluated.

Table 12 presents information on a total of 18 plates that may show an image of C/1945 X1 or its debris, including the unreduced plate AM 25208 from December 14 (Table 1) but not the five from Table 4. Because of the position uncertainties, we include plates that nominally miss the comet's position by up to 2°.5.

These are all patrol plates, with very large fields of view (Section 3). The Ross-Fecker plates (RB) cover a rectangle of 22°.32 in right ascension and 27°.90 in declination (~ 600 square degrees), the Cooke plates (AM) 34°.48 by 43°.10 (~ 1500 square degrees). The column of Table 12, titled *Plate*, shows whether the comet's predicted position, given by the standard polar coordinates relative to the plate center, is (ON) or is not (OFF) within the limits of the plate. The column *Edge* indicates the distance of the comet's predicted position from the plate edge. The smaller the number in an ON case, the more difficult it will be to identify and astrometrically evaluate the image because of optical imperfections far from the optical axis of the instrument and a potential lack of appropriate field stars. The smaller the number in an OFF case, the greater is a chance that the image could, after all, appear on the plate because of the positional uncertainties.

We list a total of seven preperihelion plates on which the comet should show up if bright enough and four such plates with the comet's predicted location barely missed; see Section 7.2 for the brightness constraints. After perihelion there are only two potentially useful plates by the

end of January to check whether any material part of the head survived; two additional plates just miss the comet's expected position. On one of the plates taken on January 21, we predict that the comet's location is not far from the center. The comet's head should also appear on five plates exposed during February (AM 25269 on the 7th, AM 25272 and AM 25273 on the 8th, RB 14224 on the 19th, and RB 14246 on the 27th), but there is no point in examining these unless the comet shows up, rather unexpectedly, on the January plates.

Finally, there is a group of three plates (footnotes *e* and *f* in Table 12), which miss the predicted position of the comet's head by a wide margin but may be relevant to a search for traces of the comet's dust debris (Section 8.2). This group includes the January 8 plate (Table 1), taken with the Ross-Fecker camera specifically for the purpose to recover C/1945 X1 (Section 3). Another plate, taken almost simultaneously with the Metcalf refractor (Table 1), is not listed, because it is deemed useless on account of its small field.

7.2. Photometry and the Light Curve

To predict the brightness of a comet is always risky, as has amply been documented by historical examples. For the Kreutz sungrazers, the task is further complicated by apparent differences between the shapes of the preperihelion light curves of a prominent Kreutz comet (observed as a bright object from the ground) and a dwarf sungrazer (observed only from *SOHO/STEREO*), as suggested by Knight et al. (2010). However, a preperihelion light curve is known for only one prominent sungrazer, C/1965 S1 (Sekana 2002).⁸ It is not advisable to generalize this light curve as a standard attribute of all bright Kreutz sungrazers. This caveat is supported by the perceived differences among the post-perihelion light curves for five prominent Kreutz objects (C/1843 D1, C/1882 R1, C/1963 R1, C/1965 S1, and C/1970 K1), which were fading with heliocentric distance at average rates from $r^{-3.3}$ to $r^{-5.1}$ (Sekana 2002).

Knight et al. (2010) concluded that the rate of brightening of the dwarf Kreutz sungrazers observed with the *SOHO* coronagraphs changes strikingly near $24 R_{\odot}$ (0.11 AU) from the Sun from $\sim r^{-7.3}$ to $\sim r^{-3.8}$; this slower rate of brightening then holds, according to them, down to $16 R_{\odot}$ (0.075 AU), where the light curve begins to flatten. They estimated that the steep rate is unlikely to persist at heliocentric distances greater than $50 R_{\odot}$ (0.23 AU) and that farther from the Sun the dwarf sungrazers brighten on their way to perihelion by again following an $r^{-3.8}$ law. However, Ye et al. (2014) suggested that there is a significant diversity in the preperihelion light curves of the dwarf Kreutz sungrazers. They called attention to either an outburst (whose amplitude exceeded 5 magnitudes) or an extremely steep brightening (r^{-11} or steeper) of a dwarf sungrazer C/2012 E2 between 1.06 AU and 0.52 AU from the Sun, while the object followed, on the average, an $\sim r^{-4}$ (or flatter) law during its approach to perihelion between at least 0.52 AU (rather

than 0.23 AU) and 0.07 AU. Ye et al. also pointed out that another dwarf Kreutz sungrazer, C/2012 U3, was not detected at a heliocentric distance of 1.31 AU before perihelion and was then much fainter than it should have been if it followed the Knight et al.'s (2010) prediction.

Very illuminating is Ye et al.'s (2014) comparison of the light curves of C/2012 U3 and C/2011 W3 (Lovejoy). Although C/2011 W3 was not a dwarf sungrazer, it brightened according to an $r^{-6.9}$ law (Sekana & Chodas 2012) from 0.75 AU down to 0.34 AU, thus behaving very differently from the prominent sungrazer C/1965 S1 ($r^{-4.1}$ between 1.02 AU and 0.03 AU; Sekana 2002). It appears that there is (i) a distinct possibility that, among the dwarf sungrazers, the steep, r^{-7} law applies to heliocentric distances of around 1 AU and possibly even further away from the Sun; and (ii) at least some of these objects appear to be subjected to outburst-like brightening at moderate distances from the Sun on their way to perihelion.

The potential implications for the brightness evolution of C/1945 X1 are obvious. A major obstacle to accepting this object as a dwarf sungrazer is its considerable brightness reported at the time of discovery. Comparison with C/2011 W3 shows that C/1945 X1 was intrinsically (i.e., after a correction has been applied for the geocentric distance) fully 4.5 magnitudes (!) *brighter* at the same heliocentric distance. Assuming the reported estimate is correct, this problem can only be overcome if one accepts that C/1945 X1 experienced a major outburst some time before the discovery, which was thereby substantially facilitated. If the amplitude of the outburst was greater than ~ 4.5 magnitudes, and therefore comparable to that of C/2012 E2, C/1945 X1 would have been fainter than C/2011 W3 before the onset of the outburst. From the standpoint of chances that C/1945 X1 could be detected on any of the pre-discovery plates in Table 12, the pivotal parameter is the time when the putative event took place. If this general scenario is correct, the comet's unusual brightness is indeed explained, but there is rather a slim chance of detecting the comet on any of the pre-outburst plates.

An alternative explanation of the reported magnitude of C/1945 X1, if it should be a dwarf sungrazer, is simply a gross overestimation of its brightness by the discoverer. In any case, these considerations show the critical need for a thorough photometric examination of the comet's Boyden images, both those from the period of December 11–15 and any pre-discovery ones.

Keeping all our options open, we illustrate the dramatic differences, over a wide range of heliocentric distances, between the C/1945 X1 brightness predictions based on the r^{-4} and r^{-7} laws by listing the apparent magnitudes in columns 8–9 of Table 11. One should, however, be able to discriminate between the two laws over a much shorter range of r . In fact, in the known Boyden images taken over the period of December 11–15, the comet should have brightened by 0.7 magnitude if the r^{-4} law applied, but by 1.3 magnitudes if the steeper law was in effect. The ephemeris suggests that C/1945 X1 might have been as bright as magnitude 15 in the second half of September, about 3 months before perihelion. In order that no image be missed, we began our search for plates that fit the predicted position of the comet as

⁸ Only a single, crude preperihelion magnitude estimate is available for C/1882 R1, the brightest Kreutz sungrazer over the past two centuries. This estimate is based on reports of its rivaling Venus in brightness at the time of discovery, 12 days before perihelion (Gould 1883).

early as mid-September, since the Ross-Fecker camera, the more powerful of the two patrol instruments, has nominally a limiting magnitude 15 as well (Section 3).

8. WHAT KIND OF A SUNGRAZER WAS C/1945 X1?

Evidence of the fate of C/1945 X1 after its passing through perihelion is vital for determining the place of this object in the hierarchy and evolution of the Kreutz system and for answering the question of whether it was a dwarf sungrazer. We propose to establish this from comparison with some better investigated sungrazers.

8.1. C/1945 X1 and the Transition Sungrazers

Based on large numbers of observations, the members of the Kreutz system are usually divided into two categories: prominent (bright and often quite spectacular as seen from the ground) and dwarf (defined in Section 1). This is a very simplistic classification, because it ignores intermediate objects, which occupy the transition between both categories and, albeit scarce, are momentous for a better understanding of the disintegration process of the Kreutz sungrazers.

In an effort to determine where C/1945 X1 is likely to fit in, we selected three “standards” to define a scale for transition objects in the order of increasing similarity to the dwarf members. The standards were chosen to be represented by C/2011 W3, C/1887 B1, and C/2007 L3. Next we describe their diagnostic properties, which will be searched for on the best suited plates of C/1945 X1 in order to classify the comet on this scale.

C/2011 W3 was the most persistent and nearest the status of a prominent member among the three objects. With a perihelion distance of $1.19 R_{\odot}$, this comet survived intact (without its nucleus disintegrating completely) until 38 ± 5 hours after perihelion, at which time it suddenly fell apart in a *terminal outburst*, losing suddenly its residual, $\sim 10^{12}$ g nucleus and head (Sekanina & Chodas 2012). The tail, made up of microscopic dust particles ejected from the nucleus *before* perihelion, was seen to survive perihelion for at least 24 hours as a *syndyname* — a locus of dust released at different times but subjected to the same radiation pressure acceleration β — of $\beta = 0.6$ the solar gravitational acceleration, typical for dielectric submicron-sized particles. Only grains ejected less than 0.1 day before perihelion, which approached the Sun within $1.8 R_{\odot}$, sublimated away. After perihelion the comet formed a new, spectacular, headless tail, most of which was a product of the event ~ 38 hours after perihelion. This tail was a *synchrone* — a locus of dust grains of different sizes (subjected to a broad range of radiation pressure accelerations), all released at the same time — that was under observation for up to 90 days, until mid-March 2012. Its representative length during most reported sightings again suggested a maximum radiation pressure acceleration of $\beta \simeq 0.6$ the solar gravitational acceleration. Only during the late observations (60–90 days after perihelion) did the visible tail consist of merely micron-sized and larger grains, whose $\beta \ll 0.6$ the solar gravitational acceleration.

C/1887 B1 is the runner-up to C/2011 W3. Available information is rather limited, because this object was discovered only after perihelion as a headless, narrow, ribbon-like tail, again a synchrone. Nonetheless, the systematic variations in this tail’s orientation with time

suggest that the nucleus survived intact until 5.8 ± 0.8 hours after perihelion (Sekanina 1984), at which point it must have suddenly disintegrated in a terminal outburst similar to that of C/2011 W3. At perihelion the comet was merely $1.04 R_{\odot}$ from the Sun (Sekanina 1978; Sekanina & Chodas 2004). The tail, truly spectacular during the early sightings from 8.5 days after perihelion on, was under observation until 18.5 days after perihelion and its length implied a maximum radiation pressure acceleration of dust particles that dropped from ~ 0.4 the solar gravitational acceleration at discovery to ~ 0.05 during the last three reported observations. The minimum particle size in the visible part of the tail was thus increasing with time from less than 1 micron to several microns.

C/2007 L3 is, of the three standards, the most remote from the prominent Kreutz-system members, being in fact a representative of a relative small group of bright dwarf Kreutz sungrazers, which develop long, extremely narrow tails upon their approach to perihelion and which we refer to hereafter as the *superdwarfs*. Like ordinary dwarf sungrazers, their nuclei fail to survive perihelion, so that they form no post-perihelion tails. We chose C/2007 L3 as a representative primarily because it was imaged by both *SOHO* and *STEREO*, unlike most of its peers. The comet had a perihelion distance of $1.530 R_{\odot}$ (Marsden 2008), very close to our best estimate for C/1945 X1, its brightness peaked at magnitude ~ 3 and its head disappeared about 80 minutes before perihelion, at a heliocentric distance of $2.75 R_{\odot}$ (Green 2007). The *SOHO* and *STEREO* images were studied in considerable detail by Thompson (2009), who closely confirmed the earlier conclusions by Sekanina (2000), based on several objects, that preperihelion images of these tails show that they are synchrones, referring to emission-shutoff times of 26 ± 7 hours before perihelion and to heliocentric distances at shutoff of $23.5 \pm 4.5 R_{\odot}$.⁹ This average agrees remarkably well with Knight et al.’s (2010) distance at which the slope of the light curves suddenly changes from -7.3 to -3.8 (Section 7.2).¹⁰ The tail of C/2007 L3 survived the comet’s perihelion, as did the preperihelion tail of C/2011 W3. Thompson examined its remnant and found, unlike Sekanina & Chodas (2012) for C/2011 W3, that the feature remained synchronic to its last examined image, nearly 17 hours after perihelion, but that its position was slightly modified by a loss of angular momentum, possibly due to atmospheric drag from the solar corona. The apparent discrepancy is explained by the fact that the dust emission of C/2011 W3 did not shut off about 1 day before perihelion, but continued. Both Sekanina (2000) and Thompson (2009) detected the maximum radiation pressure accelerations of $\beta \simeq 0.6$ the solar gravitational attraction. Comet C/2007 L3 was not the only Kreutz superdwarf whose dust tail was observed to survive perihelion. Other examples are C/1979 Q1, the first *Solwind* comet (Michels et al. 1982), C/1998 K10, one of the dozen comets examined by Sekanina (2000), etc. It is

⁹ For the best two imaged comets (C/1996 Y1 and C/1998 K10) in his set, Sekanina (2000) noticed that the tail was actually bent and, unlike its bright synchronic portion, the faint, outer part was a syndyname with a range of the ejection times.

¹⁰ This evidence may be interpreted to indicate that dust emission essentially ceases at $24 R_{\odot}$ from the Sun and the $r^{-3.8}$ law of brightening measures an effect of the object’s fragmentation.

likely that most, if not all, superdwarfs would show their tails surviving perihelion, if their images are closely analyzed. About 10 such comets from 1995–2005 in Knight et al.’s (2010) Table 2 and all 19 sungrazers from 2006–2013 in Sekanina & Kracht’s (2013) Table 1 belong to this subcategory, which is at present estimated to include about three dozen objects.

So where does C/1945 X1 fit in? Employing the constraint that no tail was ever reported with the unaided eye after perihelion, it is certain that this comet was too faint to be placed between C/2011 W3 and C/1887 B1 or even near C/1887 B1. Since a *preperihelion* tail is always found to survive for only 1 day or so after perihelion, there is no chance of detecting it on any of the plates listed in Table 12. Should we find traces of the comet’s synchronic tail, a product of a *post-perihelion* outburst, on any of these plates, then C/1945 X1 is to be classified on this three-point scale between C/1887 B1 and C/2007 L3, in which case it was a transition object more massive than a superdwarf. If not, it has to be concluded that C/1945 X1 cannot be positioned higher than C/2007 L3, so that, at best, it was a superdwarf.

8.2. Search for Traces of C/1945 X1 After Perihelion

From these considerations it follows that while a search for, and examination of, the comet’s preperihelion images on the plates listed in Table 12 should serve to improve our understanding of the comet’s orbital motion and its light curve, a careful search for traces of the comet on, and examination of, the plates taken after perihelion should provide information on the comet’s fate and help answer the question of whether C/1945 X1 was a transition object or a dwarf sungrazer; because of the lack of information on the comet’s appearance in close proximity of perihelion (Table 12), we cannot distinguish between its classification as a dwarf or a superdwarf.

Before we discuss specific search opportunities, we note that the dust released from this comet before perihelion was affected by sublimation less severely than the dust from C/2011 W3. The orbital elements for C/1945 X1’s preperihelion ejecta subjected to radiation pressure accelerations $\beta = 0.6$ the solar gravitational acceleration are summarized in Table 13. It follows that if this comet’s dust had sublimation properties similar to those of the dust from C/2011 W3, only particles ejected within ~ 1 hour of perihelion should have sublimated completely, because of a greater perihelion distance of C/1945 X1. A major delay of several days in passing through perihelion is noted as a yet another effect: for example, particles ejected 50 days before the comet’s perihelion did not reach their own perihelion until late on January 5.

As to the sources of information on comet C/1945 X1 after perihelion, a remote opportunity occurred on 1946 January 3.51 UT, the time of a solar eclipse.¹¹ Unfortunately, it was merely partial, of magnitude 0.553, and visible only from Antarctica and surrounding oceanic regions. Even less of the Sun was occulted at the locations of several permanent British scientific stations in Antarctica near the southernmost tip of South America (Operation Tabarin; e.g., Haddelsey 2014). At J. Shanklin’s suggestion we checked the UK Met Office Archives in

Table 13

Orbital Elements of Dust Particles Subjected to $\beta = 0.6$ and Ejected from Comet 1945 X1 up to Perihelion.

Time of ejection (days) ^a	Time of perihelion (days) ^a	Perihelion distance (R_{\odot})	Orbital eccentricity
−50	+8.868	3.757	1.035
−40	+7.142	3.749	1.041
−30	+5.410	3.732	1.049
−25	+4.540	3.721	1.055
−20	+3.667	3.706	1.064
−15	+2.788	3.682	1.077
−10	+1.899	3.641	1.101
−7	+1.357	3.596	1.127
−5	+0.989	3.545	1.157
−3	+0.610	3.450	1.217
−2	+0.412	3.356	1.279
−1	+0.203	3.134	1.426
−0.7	+0.136	3.027	1.527
−0.5	+0.089	2.896	1.642
−0.3	+0.041	2.673	1.861
−0.2	+0.017	2.481	2.082
−0.1	−0.004	2.144	2.567
−0.05	−0.010	1.843	3.150
−1 ^h	−0.009	1.779	3.299
0.0	0.000	1.530	4.000

^a Reckoned from the time of the comet’s perihelion passage.

Exeter and, not surprisingly, found no report on any relevant observations at the time.

Back at Boyden, an attempt was made by M. J. Bester on January 8 to recover the comet; the search, as pointed out (Sections 3 and 7.1), was conducted with the Metcalf refractor and the Ross-Fecker piggyback camera. Both exposures pointed in the same direction because they overlapped each other; the Metcalf 45 minute exposure began 20 minutes earlier and was longer by 5 minutes. The pointing of the telescope is, however, a mystery: as performed, it could not accommodate the comet’s predicted position within the limits of either plate.

January 8 was the date of publication of Cunningham’s (1946b) ephemeris, but early in the morning Bester could not have been in the possession of the official announcement from Copenhagen. Yet, the telescope was set to point precisely in accord with the ephemeris in declination and was — most peculiarly — off by exactly 2 hours to the west of the ephemeris place in right ascension. Such a coincidence surely cannot be accidental. We presume that Bester was notified directly by Cunningham ahead of the ephemeris’ publication, perhaps by cable, but there was a miscommunication, an error in one coordinate. In any event, the time of Bester’s observation was fundamentally incorrect because during the exposures the comet, less than 30° from the Sun, was below and, later, very close to the horizon. Since the comet was almost exactly south of the Sun, it could have been observed either shortly after sunset or, somewhat preferably, just before sunrise. The need to take a fairly long exposure did of course constrain the choice of the observation time. If observed at the correct time with the telescope set to point in accord with Cunningham’s ephemeris in both coordinates, the comet’s position would have been exposed on both plates, even though only ~ 0.5 from the edge of the Metcalf plate.

¹¹ See the website <http://eclipse.gsfc.nasa.gov/SEplot1901/SE1946Jan03P.GIF>.

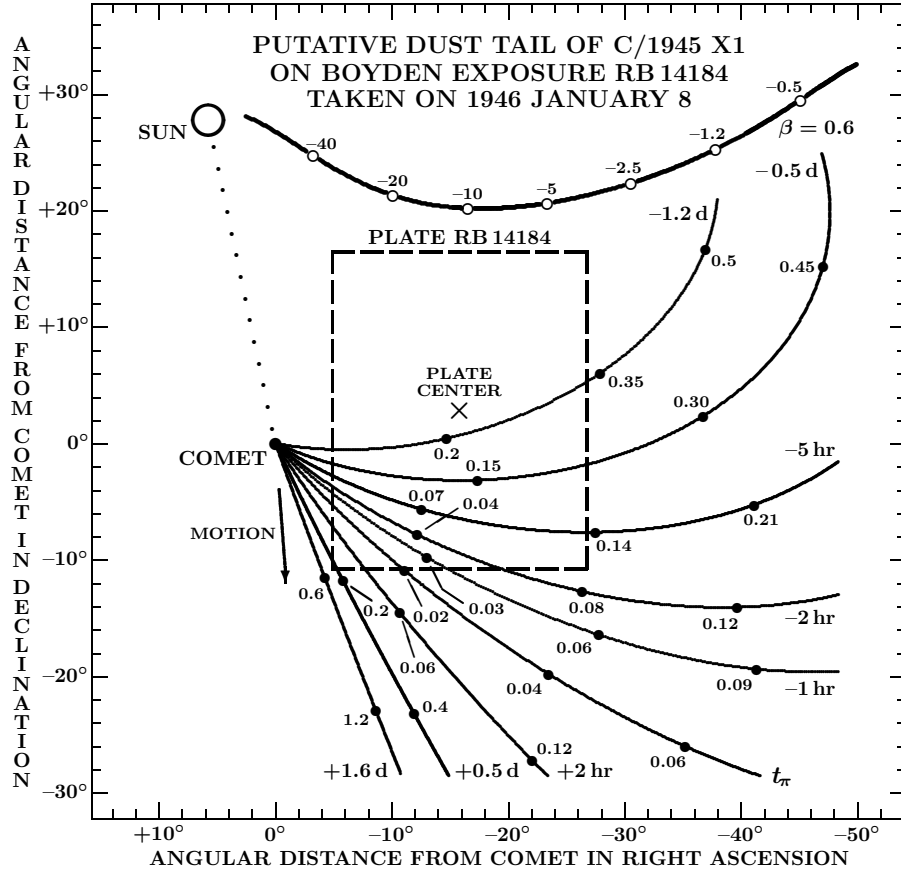


Figure 5. The predicted projected position of C/1945 X1 relative to the sky area exposed on the plate RB 14184, taken by M. J. Bester with the Ross-Fecker camera on 1946 January 8.07729 UT. While the comet's head was more than 4° off the eastern edge of the plate, much of the dust tail made up of particles released near and shortly before perihelion occupy the lower, southern part of the plate's field. Dust ejected as far back as ~ 40 days before perihelion occupies the rest of the plate. The curves to the south of the plate center are the synchrones, the loci of the dust that was ejected from the comet at particular times between 1.2 days before perihelion and 1.6 days after perihelion; the curve t_π is the perihelion synchrone. The numbers along the synchrones are the values β , the ratio between the solar radiation pressure acceleration and the solar gravitational acceleration; β and the ejection time govern the motions of the dust ejecta. Values near $\beta \approx 0.1$ are typical for micron-sized grains, those near or in excess of 0.5 refer to a variety of submicron-sized grains. The thick curve at the top, labeled $\beta = 0.6$ is a syndynome defined by this β ratio and typical for dielectric submicron-sized particles. Shown along this curve are the times of ejection in days before perihelion; see text for the significance of this syndynome.

Figure 5 displays the projected positions of the comet and the Sun relative to the pointing direction of the plate RB 14184, taken with the Ross-Fecker camera on January 8, 11 days after perihelion. Although dust ejecta are predicted to be all over the plate, their detection, contingent on the time-dependent emission rate, is problematic on account of their generally low surface brightness, except when released during a sharply peaked event, such as a terminal outburst. The curves emanating in the figure from the comet's head and distributed mostly in the lower part of the plate are the near-perihelion synchrones. Their selected range is from 1.2 days before perihelion to 1.6 days after perihelion. Few post-perihelion ejecta project onto the plate, barely touching its southeastern corner, and only a limited fraction of the perihelion ejecta crosses the plate. On the other hand, much of the dust released as far back as ~ 40 days before perihelion is projected onto the plate. We emphasized in Section 8.1 that the preperihelion tails of the transition object C/2011 W3 and of C/2007 L3 and many other (if not all) superdwarfs survived perihelion for not much longer than ~ 1 day at the most. Such features are too

close to the Sun to observe from the ground. It is only for the sake of interest that Figure 5 shows the syndynome $\beta = 0.6$, made up of dielectric submicron-sized particles ejected from C/1945 X1 before perihelion, to miss the field of the sky covered by the plate RB 14184, nearly grazing it along the entire northern edge.

The plate RB 14184 may prove useful. If C/1945 X1 experienced a terminal outburst and disintegrated within an hour or two after perihelion and if the ejecta contained a large abundance of grains several microns in diameter, there is a possibility that this debris could show up as a band of light across the lower left corner of the plate. The phase angles favor a modest forward-scattering effect, being mostly in a range of 100° – 110° . Submicron-sized ejecta released from the comet at the same times should miss the plate. Thus, a detection or nondetection of a post-perihelion synchronic tail could provide meaningful constraints on the existence of a terminal outburst and on the time of nucleus disintegration.

We found two more plates that might provide additional limited information on a potential post-perihelion terminal outburst: AM 25231, taken with the Cooke lens

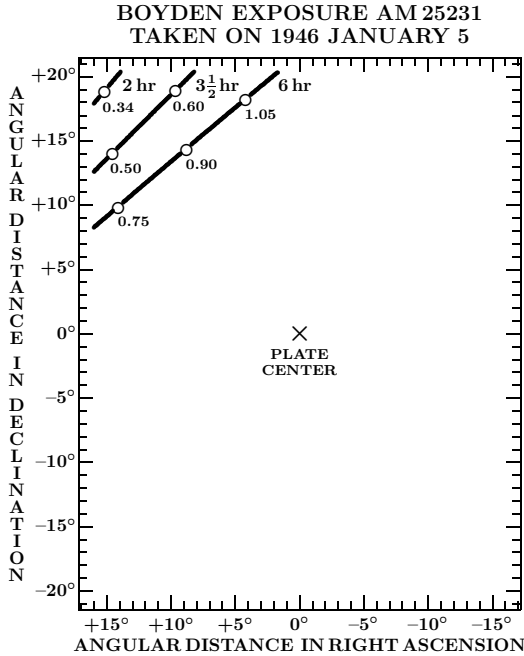


Figure 6. Predicted positions, on a Cooke plate AM25231 taken on January 5.04600 UT, of synchrones that depict C/1945 X1’s dust ejecta from hypothetical terminal outbursts 2, 3.5, and 6 hours after perihelion. The smaller-font digits refer to particles subjected to a variety of radiation pressure accelerations β between 0.34 and 1.05 the solar gravitational acceleration. Since the Kreutz comets appear to have $\beta \leq 0.6$, only outbursts that occurred between ~ 2 and ~ 4 hours after perihelion might be detected on this plate.

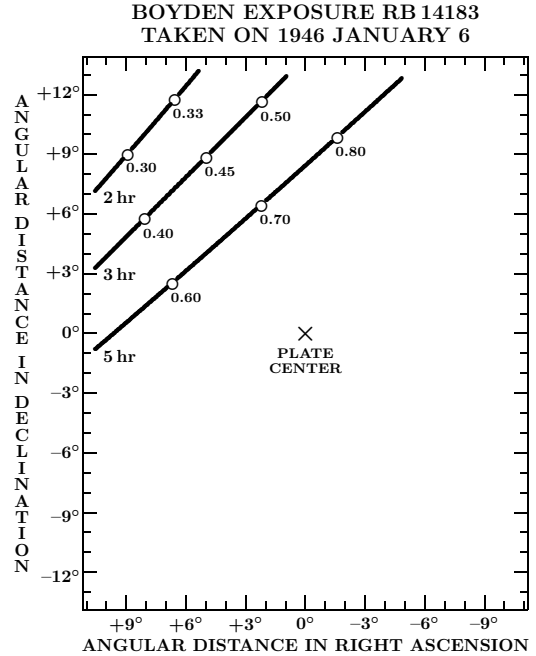


Figure 7. Predicted positions, on a Ross-Fecker plate RB14183 taken on January 6.04985 UT, of synchrones depicting the comet’s dust ejecta from hypothetical terminal outbursts 2, 3, and 5 hours after perihelion. The smaller-font digits refer to particles subjected to a variety of radiation pressure accelerations β between 0.3 and 0.8 the solar gravitational acceleration. Since the Kreutz comets appear to have $\beta \leq 0.6$, only outbursts that occurred between ~ 1 and ~ 5 hours after perihelion might be detected on this plate.

in the morning of January 5, and RB14183, taken with the Ross-Fecker camera 24 hours later. They both are listed in Table 12. The synchrones for the January 5 plate are depicted in Figure 6, those for the January 6 plate in Figure 7. The positions of dust particles relative to the comet’s nucleus, determined by a computer code in terms of their polar coordinates, were converted to the polar coordinates of the offsets from the plate center, using a technique described in some detail in the Appendix. An advantage of these plates relative to that on RB14184 is their exposure times, 115 and 90 minutes, respectively, as opposed to only 40 minutes (Table 12). The January 5 plate might provide useful information only if the terminal outburst took place between, at most, ~ 2 and ~ 4 hours after perihelion; a synchronic tail containing earlier ejecta would miss this plate, while segments of later synchrones limited to $\beta > 0.6$ the solar gravitational acceleration are unlikely to refer to any real tails (Section 8.1). Similarly, the January 6 plate might provide information only on an outburst that occurred between ~ 1 and ~ 5 hours after perihelion. No forward-scattering effect can be expected in either case, as the phase angles range between about 60° and 80° .

In the highly unlikely case that a major fragment of the original nucleus survived for weeks after perihelion, the best search opportunity is offered by a Cooke plate AM25241, taken on January 21, on which the comet is predicted to be less than 7° from the center (Table 12). Less favorable circumstances should accompany a search on a plate AM25260, taken 9 days later, on which the comet’s predicted position is only $2^\circ.5$ from the edge. Additional search opportunities are more discouraging still.

9. CONCLUSIONS

Comet C/1945 X1 has been rather an oddball among the Kreutz sungrazers observed from the ground ever since its discovery 70 years ago. Although the dilatory handling of the Boyden plates contributed to the snail pace in getting out the facts about the object, it was nonetheless its apparent lack of luster near and after perihelion that is primarily responsible for our ignorance of its properties, fate, and place in the Kreutz system.

The comet’s disappointing post-perihelion performance — especially the absence of a prominent dust tail — provides a strong argument against its being on a par with the headless sungrazers C/2011 W3 and C/1887 B1 that survived perihelion with a fairly massive nucleus intact but disintegrated shortly afterwards. The plausible scenarios for C/1945 X1 are thus limited to two: either the comet’s surviving mass was sufficient to generate a modest, but not spectacular, post-perihelion tail, or the comet completely disintegrated still before perihelion. While there is not much of a difference between the two scenarios, we use the second one to define a dwarf Kreutz sungrazer. The existence of a terminal outburst is therefore critical to distinguish between the two options.

Taking account of the indirect planetary perturbations on the premise that a precursor of C/1945 X1 separated from its common parent with C/1882 R1 (Sekanina & Chodas 2004), we determine that the line of apsides of C/1945 X1 should point toward an ecliptical longitude of $L_\pi = 282^\circ.44$ and latitude of $B_\pi = +35^\circ.16$ (Equinox J2000) and that the comet’s osculating semimajor axis a should be 96.70 AU at an epoch 1945 December 28.0 TT or 96.67 AU at an epoch December 11.0 TT.

Employing this value of a as an orbital constraint, our *Best Fit* purely gravitational solution based on all five observations left an unacceptably large offset of $0^\circ.57$ from the nominal apsidal-line direction, apparently because the third observation was inferior. This was confirmed by four-observation gravitational solutions, of which the one based on the positions from December 11, 12, 14, and 15 was by far the most promising, leaving an offset from the nominal apsidal-line direction of $0^\circ.08$, much better but still not entirely satisfactory.

Applying a technique introduced recently by us in Paper 1, we show that the incorporation of a nongravitational acceleration of the orbital motion improves the fit in terms of both the apsidal-line offset and mean residual. Use of Marsden et al.'s (1973) standard formalism suggests an acceleration on the order of 10^{-6} AU day $^{-2}$ (with a relative error of ± 8 – 17%), near the lower end of a range typical for the dwarf sungrazers. A preferable nongravitational model, based on a much steeper acceleration law (apparently common among the dwarf sungrazers; see Paper 1) than is the standard law, leads to the same magnitude of the integrated effect but fits the observations better, with the relative errors of the nongravitational parameters reduced to ± 5 – 7% .

In order to augment the current, very limited data set, an extensive search for further possible images of the comet should be undertaken. We hope to be able to conduct such a search, based on our orbital computations suggesting that at least 7 and perhaps as many as 11 preperihelion Boyden patrol plates taken between late September and mid-December may contain such images. The plates will be inspected in the near future, once their digitized copies are made available by the DASCH Project. At present we do not anticipate to expand our search to archives of wide-field plates from other observatories (e.g., Tsvetkov & Tsvetkova 2012).

In addition to positional data of the comet, its photometry will also have to be performed to reexamine the reported brightness at discovery and to settle the issues of the rate of brightness variations with heliocentric distance and the chance of an early preperihelion outburst. Comparison with C/2011 W3 and C/2012 E2, among others, may help settle some of the issues of preperihelion activity of the Kreutz sungrazers.

Finally, to pursue a solution to the complex problem of C/1945 X1's place in the hierarchy of the Kreutz system and the comet's fate, we also will examine some post-perihelion Boyden patrol plates to search for both potential relics of the comet itself and/or possible traces of its dust tail as a product of a modest terminal outburst that may have occurred just hours past perihelion. Whereas it appears that, masswise, C/1945 X1 could not compete with either C/2011 W3 or C/1887 B1, we will try to disentangle a mystery of whether it still could be considered a transition object distinctly more massive than a superdwarf, such as C/2007 L3, C/1998 K10, or C/1979 Q1, or it does not differ materially from the Kreutz dwarfs or superdwarfs — and thus answer the cardinal question posed in this paper's title.

The authors thank D. van Jaarsveldt, J. Grindlay, A. Doane, and E. Los for their information on the observers and the plate collection from the Boyden Station and on the Harvard College Observatory's DASCH Project.

This research was carried out in part at the Jet Propulsion Laboratory, California Institute of Technology, under contract with the National Aeronautics and Space Administration.

APPENDIX

TRANSFORMATION OF DUST PARTICLE POSITION FROM COMETOCENTRIC TO PLATE CENTER COORDINATES

The code computing the position of a dust particle, which is a function of the ejection time, t_{eject} , and a ratio of the radiation pressure acceleration to the solar gravitational acceleration, β , provides the polar coordinates in reference to the comet's nucleus in projection onto the plane of the sky — the angular distance from the nucleus, $D_*(t_{\text{eject}}, \beta)$, and the position angle, $\Pi_*(t_{\text{eject}}, \beta)$, reckoned from the north through the east. The equatorial coordinates of the nucleus, right ascension α_0 and declination δ_0 , and the coordinates of a particle, $\alpha_*(t_{\text{eject}}, \beta)$ and $\delta_*(t_{\text{eject}}, \beta)$, are related to D_* and Π_* by the well-known expressions,

$$\begin{aligned} \cos D_* &= \sin \delta_0 \sin \delta_* + \cos \delta_0 \cos \delta_* \cos \Delta\alpha_*, \\ \cot \Pi_* &= \cos \delta_0 \tan \delta_* \csc \Delta\alpha_* - \sin \delta_0 \cot \Delta\alpha_*, \end{aligned} \quad (19)$$

where $\Delta\alpha_* = \alpha_* - \alpha_0$. To convert the particle's position from the cometocentric coordinate system to the coordinate system centered on the center of a plate, we first compute right ascension α_* and declination δ_* of the particle from the formulas

$$\tan \Delta\alpha_* = \frac{\sin^2 D_* \tan \Pi_* (\sin \delta_0 + \cot D_* \cos \delta_0 \sec \Pi_*)}{\cos^2 D_* (1 + \cos^2 \delta_0 \tan^2 \Pi_*) - \sin^2 \delta_0}, \quad (20)$$

and

$$\tan \delta_* = \cos \Delta\alpha_* \tan \delta_0 (1 + \cot \Pi_* \tan \Delta\alpha_* \csc \delta_0). \quad (21)$$

Since the sign of $\cos \Delta\alpha_*$ has a direct effect on the sign of $\tan \delta_*$ and therefore also on the signs of $\sin \delta_*$ and $\cos D_*$, the quadrant of $\Delta\alpha_*$ in Equation (20) needs to be chosen such that after inserting the values of $\Delta\alpha_*$ and δ_* from (21) into the first equation of (19) one gets the correct value of D_* and not its supplement.

Next, identifying α_0 and δ_0 with the coordinates of the plate center, rather than the comet's nucleus, and inserting them together with the particle's coordinates α_* and δ_* into Equations (19), one obtains an angular distance \bar{D}_* and a position angle $\bar{\Pi}_*$ that determine the particle's position relative to the plate center.

REFERENCES

- Brueckner, G. E., Howard, R. A., Koomen, M. J., et al. 1995, *Sol. Phys.*, 162, 357
 Cooper, T. P. 2003, *MNASSA*, 62, 170
 Cooper, T. P. 2005, *MNASSA*, 64, 118
 Cunningham, L. E. 1946a, *HAC*, 733
 Cunningham, L. E. 1946b, *IAUC*, 1025
 Gould, B. A. 1883, *Astron. Nachr.*, 104, 129
 Green, D. W. E. 2007, *IAUC*, 8883
 Grindlay, J., Tang, S., Los, E., & Servillat, M. 2012, *IAU Symp.*, 285, 29
 Haddelsey, S. 2014, *Operation Tabarin: Britain's Secret Wartime Expedition to Antarctica 1944–1946*. History Press, Stroud, UK
 Hockey, T. 2009, *BAAS*, 41, 572
 Howard, R. A., Moses, J. D., Vourlidis, A., et al. 2008, *Space Sci. Rev.*, 136, 67

- Knight, M. M., A'Hearn, M. F., Biesecker, D. A., et al. 2010, *AJ*, 139, 926
- Kreutz, H. 1888, *Publ. Sternw. Kiel*, 3
- Kreutz, H. 1891, *Publ. Sternw. Kiel*, 6
- Kreutz, H. 1901, *Astron. Abh.*, 1, 1
- Marsden, B. G. 1967, *AJ*, 72, 1170
- Marsden, B. G. 1989, *AJ*, 98, 2306
- Marsden, B. G. 2008, *MPEC 2008-G44*
- Marsden, B. G., & Williams, G. V. 2008, *Catalogue of Cometary Orbits 2008*, p. 108 (17th ed.; Cambridge, MA: Smithsonian Astrophysical Observatory, 195pp)
- Marsden, B. G., Sekanina, Z., & Yeomans, D. K. 1973, *AJ*, 78, 211
- Michels, D. J., Sheeley, N. R., Howard, R. A., & Koomen, M. J. 1982, *Science*, 215, 1097
- Nagahara, H., Mysen, B. O., & Kushiro, I. 1994, *Geochim. Cosmochim. Acta*, 58, 1951
- Paraskevopoulos, J. S. 1945, *IAUC*, 1024
- Pasachoff, J. M., Rušin, V., Druckmüller, M., et al. 2009, *ApJ*, 702, 1297
- Sekanina, Z. 1978, *QJRAS*, 19, 52, 57
- Sekanina, Z. 1982, *AJ*, 87, 1059
- Sekanina, Z. 1984, *Icarus*, 58, 81
- Sekanina, Z. 2000, *ApJ*, 545, L69
- Sekanina, Z. 2002, *ApJ*, 566, 577
- Sekanina, Z., & Chodas, P. W. 2002, *ApJ*, 581, 760
- Sekanina, Z., & Chodas, P. W. 2004, *ApJ*, 607, 620
- Sekanina, Z., & Chodas, P. W. 2007, *ApJ*, 663, 657
- Sekanina, Z., & Chodas, P. W. 2012, *ApJ*, 757, 127 (33pp)
- Sekanina, Z., & Kracht, R. 2013, *ApJ*, 778, 24 (13pp)
- Sekanina, Z., & Kracht, R. 2015, *ApJ*, 801, 135 (19pp)
- Simcoe, R. J., Grindlay, J. E., Los, E. J., et al. 2006, in *Applications of Digital Image Processing XXIX*, ed. A. G. Tescher, Proc. SPIE, vol. 6312, 631217 (Bellington, WA).
- Thompson, W. T. 2009, *Icarus*, 200, 351
- Tsvetkov, M., & Tsvetkova, K. 2012, *IAU Symp.*, 285, 417
- van Heerden, H. J. 2008, *MNASSA*, 67, 116
- Ye, Q.-Z., Hui, M.-T., Kracht, R., & Wiegert, P. A. 2014, *ApJ*, 796, 83 (8pp)